Electronic Supplementary Information File

Spectro-electrochemical assessments of DNA / BSA interactions, Cytotoxicity, Radical scavenging and Pharmacological implications of Bio-sensitive and Biologically active Morpholine based Metal(II) complexes: A combined experimental and computational investigation

Karunganathan Sakthikumar[a], Rajadurai Vijay Solomon[b] and Jeyaraj Dhaveethu Raja[c]*

[a]*Chemistry Research Centre, Mohamed Sathak Engineering College, Kilakarai, Ramanathapuram 623 806, Tamilnadu, India*

[b]*Department of Chemistry, Madras Christian College (Autonomous), Tambaram East, Chennai 600 059, Tamil Nadu, India*

[c]*Department of Chemistry, The American College (Autonomous), Madurai 625 002, Tamil Nadu, India*

*****Correspondence should be addressed to Jeyaraj Dhaveethu Raja:jdrajapriya@gmail.com

*****Corresponding author:

Dr. J. Dhaveethu Raja,

Associate Professor, Department of Chemistry,

The American College (Autonomous),

Madurai 625 002, Tamil Nadu, India, Tamil Nadu, India.

Email: jdrajapriya@gmail.com,

Phone: +91 94876 82202; +91 90925 61924

Table S1 Analytical and physical data of the ligand (**HL**) and its complexes (**1-5**).

Compounds (Formula Weight & Empirical Formula)	Colour	Yield (%)	M.P (˚C)	Found (Calcd) (%)				$\wedge_m$
				C	H	N	M	
(**HL**) Ligand (313.21) ($C_{13}H_{17}N_2BrO_2$)	Yellow	85.24	61	49.88 (49.80)	05.50 (05.42)	08.97 (08.93)	----	20.90
(**1**) [Cu(L)(AcO)].H_2O (452.75) ($C_{15}H_{21}N_2BrO_5$)Cu	Brownish green	80.10	92	40.03 (39.75)	04.68 (04.63)	06.25 (06.18)	14.05 (14.03)	38.90
(**2**) [Co(L)(AcO)].$4H_2O$ (502.14) ($C_{15}H_{27}N_2BrO_8$)Co	Dark blue	79.08	265	35.80 (35.84)	05.50 (05.37)	05.55 (05.57)	11.70 (11.73)	46.32
(**3**) [Mn(L)(AcO)].$4H_2O$ (498.15) ($C_{15}H_{27}N_2BrO_8$)Mn	Brown	76.92	110	36.10 (36.13)	05.57 (05.42)	05.65 (05.62)	11.05 (11.02)	48.42
(**4**) [Ni(L)(AcO)].$4H_2O$ (501.91) ($C_{15}H_{27}N_2BrO_8$)Ni	Greenish brown	75.85	245	35.83 (35.86)	05.45 (05.37)	05.59 (05.57)	11.72 (11.69)	42.30
(**5**) [Zn(L)(AcO)].$2H_2O$ (472.58) ($C_{15}H_{23}N_2BrO_6$)Zn	Reddish yellow	78.43	252	38.10 (38.08)	04.90 (04.86)	05.96 (05.92)	13.85 (13.83)	32.16

$\wedge_m$ → Molar Conductance ($Ohm^{-1}cm^2\,mol^{-1}$)

Synthesis of Schiff base ligand (HL)

The Schiff base ligand (**HL**) was synthesized by stirring an equal molar quantities (0.01 M) of 4-(2-amino ethyl)-Morpholine and 5-bromosalicyladehyde (0.01 M) in methanol (30 ml) and yellow precipitate was obtained after refluxing for two hours and the volume of the solution was reduced to one-third on water bath and cooled at room temperature. The collected pure yellow solid ligand was dried slowly at room temperature in vacuum desiccators over anhydrous $CaCl_2$. The yield of the isolated ligand (**HL**) was found to be 85.24% (Scheme 1).

Synthesis of complexes (1-5)

A solution of 2-(-(2-Morpholinoethylimino) methyl)-4-bromophenol Schiff base ligand (**HL**) (0.001 M) in methanol (40 mL) was mixed slowly to a solution of Metal(II) acetate (0.001 M) [$Cu^{II}(OAc)_2.H_2O$, $Co^{II}(OAc)_2.4H_2O$, $Mn^{II}(OAc)_2.4H_2O$, $Ni^{II}(OAc)_2.4H_2O$ and $Zn^{II}(OAc)_2.2H_2O$] in 30 mL of absolute methanol and refluxed for 3 hours after stirring for 30 minutes. The finally formed solid product was separated by filtration and purified by recrystallization using the solvent mixture of methanol-petroleum ether. Trace of water and solvents were recovered by keeping in vacuum desiccators over anhydrous calcium chloride. The synthesis of complexes (**1-5**) was followed by the similar methods and the yield was found to be 75.85 – 80.10 %. The observed molar conductivity values of complexes (**1-5**) were found in the range from 32.16 to 48.42 ohm^{-1} cm^2 mol^{-1} which was higher as compared to free ligand (20.90 ohm^{-1} cm^2 mol^{-1}) and shows that they are non electrolytic nature due to lack of dissociation. The various analytical and physical data of schiff base ligand (**HL**) and its complexes (**1-5**) were summarized in table S1 and listed as follows.

2-(-(2-Morpholinoethylimino) methyl)-4-bromophenol Ligand (HL)

Yield 85.24 %, yellow solid, m.p.61 °C. FT-IR spectrum, KBr, ν, cm^{-1}: 1639 (H-C=N-), 1273 (C-O_{Ar}), 1353 (C-N-C), 1179, 1108 (C-O-C), 2978 (C-H_{Ar}), 2939 (C-H), 2860 (H-C=N-), 3653 (-OH_{Ar}). ^{1}H NMR spectrum (300 MHz, $CDCl_3$, δ / ppm): 13.47 (1H, s, (-OH_{Ar}), 6.84 - 7.36 (3H, m, C-H_{Ar}), 8.28 (1H, s, -HC=N-), 3.74 (4H, t, -O-CH_2), 2.63 (4H, t, -N-CH_2), 2.51 (2H, p, -CH_2-CH_2,). ^{13}C NMR spectrum (400MHz, $CDCl_3$ at room temperature, ppm): 164.43 (H<u>C</u>=N-), 160.37 (<u>C</u>$_{Ar}$-OH), 134.93 (Br-C=<u>C</u>H$_{Ar}$), 133.34 (Br-C-<u>C</u>H$_{Ar}$), 120.11 (<u>C</u>$_{Ar}$-HC=N-), 119.12 (<u>C</u>$_{Ar}$=C-OH), 109.94 (Br-<u>C</u>$_{Ar}$), 76.75-77.38 (<u>C</u>DCl_3–solvent peaks), 66.93 (morpholinic-<u>C</u>H_2-O-<u>C</u>H_2), 56.60, 56.80 (morpholinic-<u>C</u>H_2-N-<u>C</u>H_2), 58.87 (=N-CH_2-<u>C</u>H_2-N),

53.83, 53.28 (=N-$\underline{C}H_2$-CH_2-N). UV-vis spectrum, Me-OH, λ_{max}, nm (cm^{-1}): 382 (26,178), 297 (33,670), 267 (37,453). Molar Conductance ($10^3\mu M$), Me-OH, $\wedge_m$, $ohm^{-1}cm^2\ mol^{-1}$: 20.90. LC-MS Mass (*m/z*), Found: 313.30 (M). Anal.Cacld (%) for $C_{13}H_{17}N_2BrO_2$: C, 49.80; H, 05.42; N, 08.93. Found (%): C, 49.88; H, 05.50; N, 08.97.

[Cu^{II}(L)AcO].H_2O Complex (1)

Yield: 80.10 %, Brownish green solid, m.p.92 °C. FT-IR spectrum, KBr, ν, cm^{-1}: 1627 (H-C=N-), 1295 (C-O_{Ar}), 1338 (C-N-C), 1179, 1108 (C-O-C), 2971 (C-H_{Ar}), 2926 (C-H), 2868 (H-C=N-), 1655, 1393 (Acetate C=O), 3423, 830 (H-O-H), 457 (M-N), 544 (M-O). UV-vis spectrum, Me-OH, λ_{max}, nm (cm^{-1}): 643 (15,552), 405 (24,691), 357 (28,011), 283(35,335). Molar Conductance (10^3 μM), Me-OH, $\wedge_m$, $ohm^{-1}cm^2\ mol^{-1}$: 38.90. μ_{eff}, BM: 1.85. LC-MS Mass (*m/z*), Found: 435.50 (M+1). Anal.Cacld (%) for $CuC_{15}H_{21}N_2BrO_5$: C, 39.75; H, 04.63; N, 06.18; Cu, 14.03. Found (%): C, 40.03; H, 04.68; N, 06.25; Cu, 14.05.

[Co^{II}(L)AcO].$4H_2O$ Complex (2)

Yield: 79.08 %, Dark blue solid, m.p.265 °C. FT-IR spectrum, KBr, ν, cm^{-1}:1631 (H-C=N-), 1306 (C-O_{Ar}), 1336 (C-N-C), 1173, 1110 (C-O-C), 2972 (C-H_{Ar}), 2923 (C-H), 2852 (H-C=N-), 1646, 1393 (Acetate C=O), 3447, 829 (H-O-H), 458 (M-N), 521 (M-O). UV-vis spectrum, Me-OH, λ_{max}, nm (cm^{-1}): 664 (15,060), 466 (21,459), 351 (28,490), 282 (35,461). Molar Conductance (10^3 μM), Me-OH, $\wedge_m$, $ohm^{-1}cm^2\ mol^{-1}$: 46.32. μ_{eff}, BM: 4.22. LC-MS Mass (m/z), Found: 431.2 (M+1). Anal.Cacld (%) for $CoC_{15}H_{27}N_2BrO_8$: C, 35.84; H, 05.57; N, 05.57; Co, 11.73. Found (%): C, 35.80; H, 05.60; N, 05.55; Co, 11.70.

[Mn^{II}(L)AcO].$4H_2O$ Complex (3)

Yield: 76.92 %, Brown solid, m.p.110 °C. FT-IR spectrum, KBr, ν, cm^{-1}: 1626 (H-C=N-), 1303 (C-O_{Ar}), 1342 (C-N-C), 1172, 1113 (C-O-C), 2975 (C-H_{Ar}), 2925 (C-H), 2858 (H-C=N-), 1648, 1394 (Acetate C=O), 3438, 823 (H-O-H), 452 (M-N), 517 (M-O). UV-vis spectrum, Me-OH, λ_{max}, nm (cm^{-1}): 396 (25,252), 380 (26,315), 272 (36,764). Molar Conductance (10^3μM), Me-OH, $\wedge_m$, $ohm^{-1}cm^2$ mol^{-1}: 48.42. μ_{eff}, BM: 1.77. LC-MS Mass (m/z), Found: 427.1 (M+1). Anal.Cacld (%) for $MnC_{15}H_{27}N_2BrO_8$: C, 36.13; H, 05.62; N, 05.62; Mn, 11.02. Found (%): C, 36.10; H, 05.67; N, 05.65; Mn, 11.05.

$[Ni^{II}(L)AcO].4H_2O$ Complex (4)

Yield: 75.85 %, Greenish brown solid, m.p. 245 °C. FTIR spectrum, KBr, ν, cm^{-1}:1623 (H-C=N-), 1306 (C-O_{Ar}), 1330 (C-N-C),1195, 1114 (C-O-C), 2973 (C-H_{Ar}), 2924 (C-H), 2860 (H-C=N-),1646, 1393 (Acetate C=O), 3438, 830 (H-O-H), 456 (M-N), 534 (M-O). UV-vis spectrum, Me-OH, λ_{max}, nm (cm^{-1}): 691 (14,471), 492 (20,325), 382 (26,178), 273 (36,630). Molar Conductance (10^3μM), Me-OH, $\wedge_m$, $ohm^{-1}cm^2$ mol^{-1}: 42.30. μ_{eff}, BM: 00. LC-MS Mass (m/z), Found: 430.1 (M+1). Anal.Cacld (%) for $NiC_{15}H_{27}N_2BrO_8$: C, 35.86; H, 05.57; N, 05.57; Ni, 11.72. Found (%): C, 35.83; H, 05.55; N, 05.59; Ni, 11.72.

$[Zn^{II}(L)AcO].2H_2O$ Complex (5)

Yield: 78.43 %, Reddish yellow solid, m.p.252 °C. FT-IR spectrum, KBr, ν, cm^{-1}: 1622 (H-C=N-), 1308 (C-O_{Ar}), 1332 (C-N-C), 1178, 1115 (C-O-C), 2968 (C-H_{Ar}), 2939 (C-H), 2861 (H-C=N-), 1648,1388 (Acetate C=O), 3431, 842 (H-O-H), 465 (M-N), 542 (M-O). ^{1}H NMR spectrum (300 MHz, $CDCl_3$, δ / ppm): 8.86 (1H, s, -HC=N-), 6.86-7.38 (3H, m, C-H_{Ar}), 3.75 (4H, t, -O-CH_2), 2.98 (4H, t, -N-CH_2), 2.53 (2H, p, -CH_2-CH_2,), 2.029 (3H, s, CH_3COO), 1.78 (b, 2H, H_2O). Molar Conductance (10^3 μM), Me-OH, $\wedge_m$, $ohm^{-1}cm^2$ mol^{-1}: 32.16. μ_{eff}, BM:

00. LC-MS Mass (m/z), Found: 437.1 (M+1). Anal.Cacld (%) for $ZnC_{15}H_{23}N_2BrO_6$: C, 56.50; H, 05.58; N, 09.76; Zn, 11.40. Found (%): C, 56.66; H, 05.48; N, 09.84; Zn, 11.35.

LC-MS mass spectra

In their LC-MS mass spectra, all complexes showed relatively intense molecular ion peaks (*m/z)* proposed to $[M(L)(AcO)].nH_2O$.[1, 2] The peaks corresponding to stepwise elimination of aryl groups are interpreted in the mass spectra of the complexes (**1-5**). Ligand (**HL**) shows the molecular ion peak at *m/z* 313.3 (M) corresponding to $[C_{13}H_{17}N_2BrO_2]^+$ and other fragmented molecular ion peaks are found at 215.0 (M+2) $[C_8H_8NBrO^+]$, 181.8 (M-1) $[C_8H_7NBr]^+$, 114.2 (M) $[C_6H_{12}NO]^+$, 100.2 (M) $[C_5H_{10}NO]^+$ and 57.1 (M+1) $[C_2H_4N_2]^+$ (Fig. S1). Complex (**1**) molecular ion peak at *m/z* 435.5 (M+1) corresponding to $[C_{15}H_{19}N_2BrO_4Cu]^+$ and other fragmented molecular ion peaks are found at 374.3 (M-2) $[C_{15}H_{19}N_2BrO_4]^+$, 317.4 (M-4) $[C_{13}H_{17}N_2BrO_2]^+$, 274.4 (M-2) $[C_8H_6BrO_2Cu]^+$, 220.3 (M+1) $[C_6H_4BrCu]^{2+}$ and 157.3 (M+1) $[C_6H_4Br]^+$ (Fig. S2). Complex (**2**) molecular ion peak at *m/z* 431.2 (M+1) relevant to $[C_{15}H_{19}N_2BrO_4Co]^+$ and other fragmented molecular ion peaks are found at 414.2 (M-1) $[C_{14}H_{16}N_2BrO_4]^+$, 371.3 (M) $[C_{15}H_{19}N_2BrO_4]^+$, 343.3 (M+1) $[C_{15}H_{22}N_2BrO_2]^+$, 274.3 (M+1) $[C_8H_6O_2BrCo]^+$ (Fig. S3). Similarly Complexes (**3**) and (**4**) show that the molecular ion peaks at *m/z* 427.1 (M+1) $[C_{15}H_{19}N_2BrO_4Mn]^+$ and 429.9 (M+1) $[C_{15}H_{19}N_2BrO_4Ni]^+$ respectively. Complex (**5**) molecular ion peak at *m/z* 437.1 (M+1) corresponding to $[C_{15}H_{19}N_2BrO_4Zn]^+$ and other fragmented molecular ion peaks are found at 372.20 (M+1) $[C_{15}H_{19}N_2BrO_4]^+$, 326.6 (M-1) $[C_{14}H_{19}N_2BrO_2]^+$, 313.3 (M+1) $[C_{13}H_{16}N_2BrO_2]^+$, 279.3 (M+1) $[C_8H_6O_2BrZn]^+$ (Fig. S4) and other peaks are followed by fragmented molecular ion of ligand (**HL**).

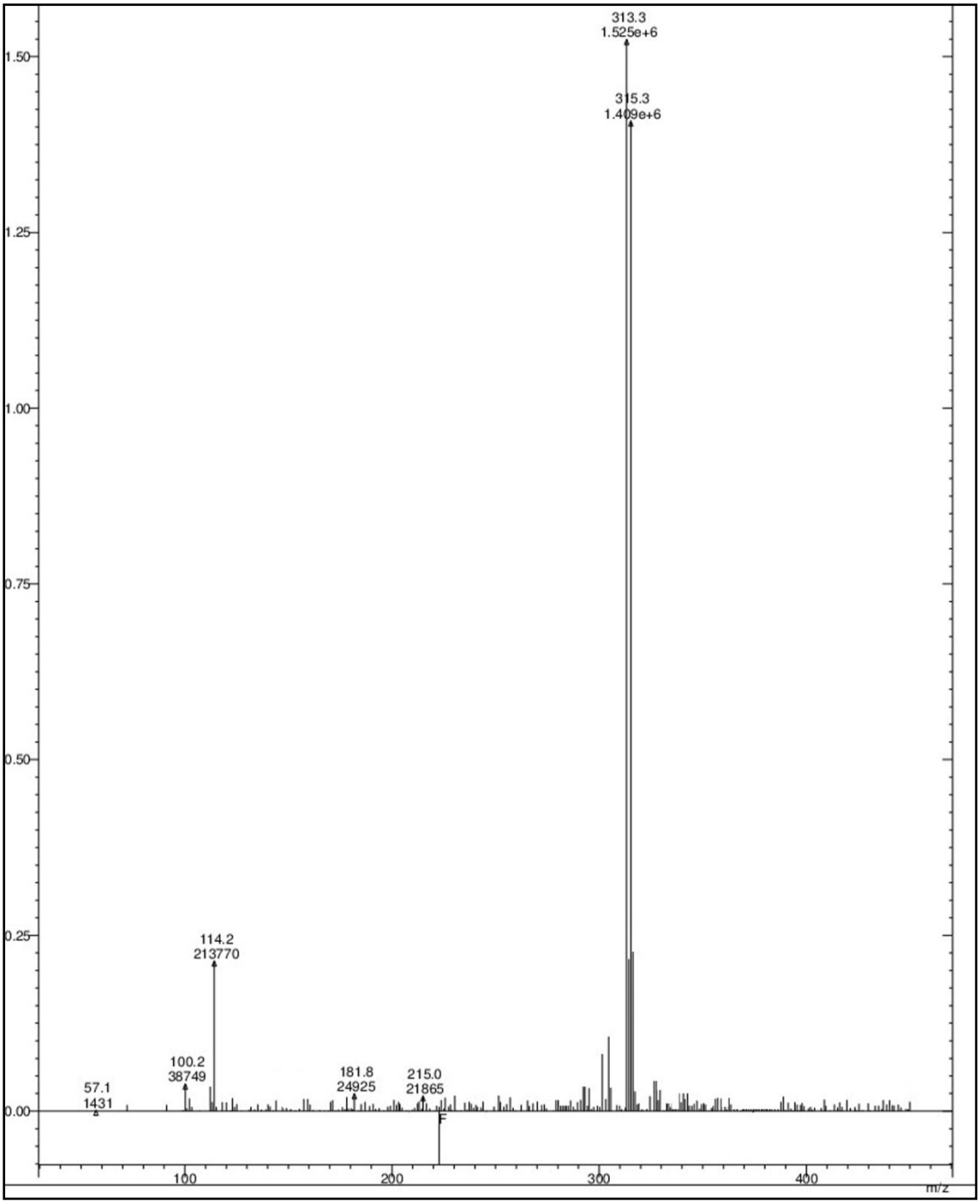

Fig. S1 LC-MS Mass spectrum of ligand (**HL**).

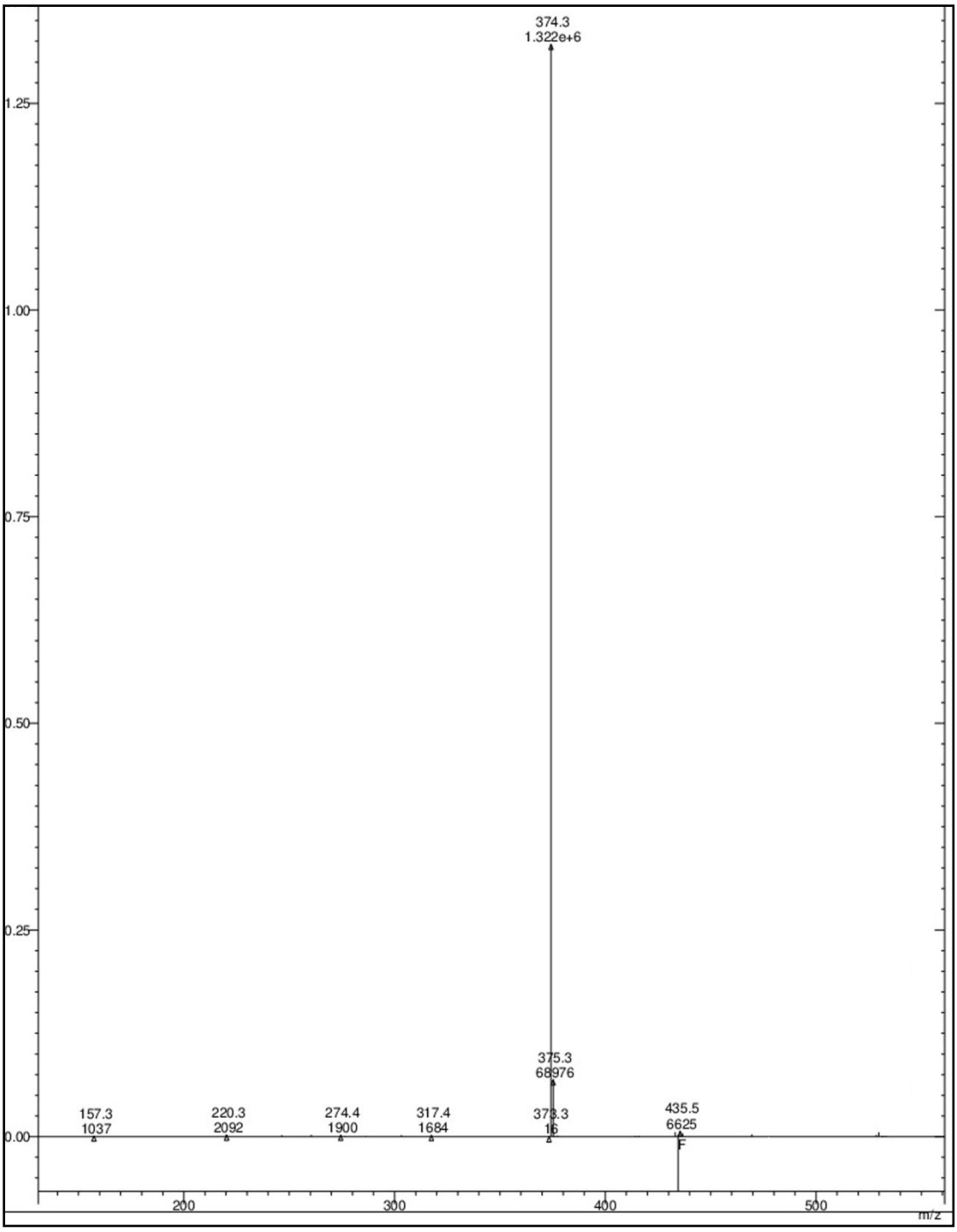

Fig. S2 LC-MS Mass spectrum of complex (**1**).

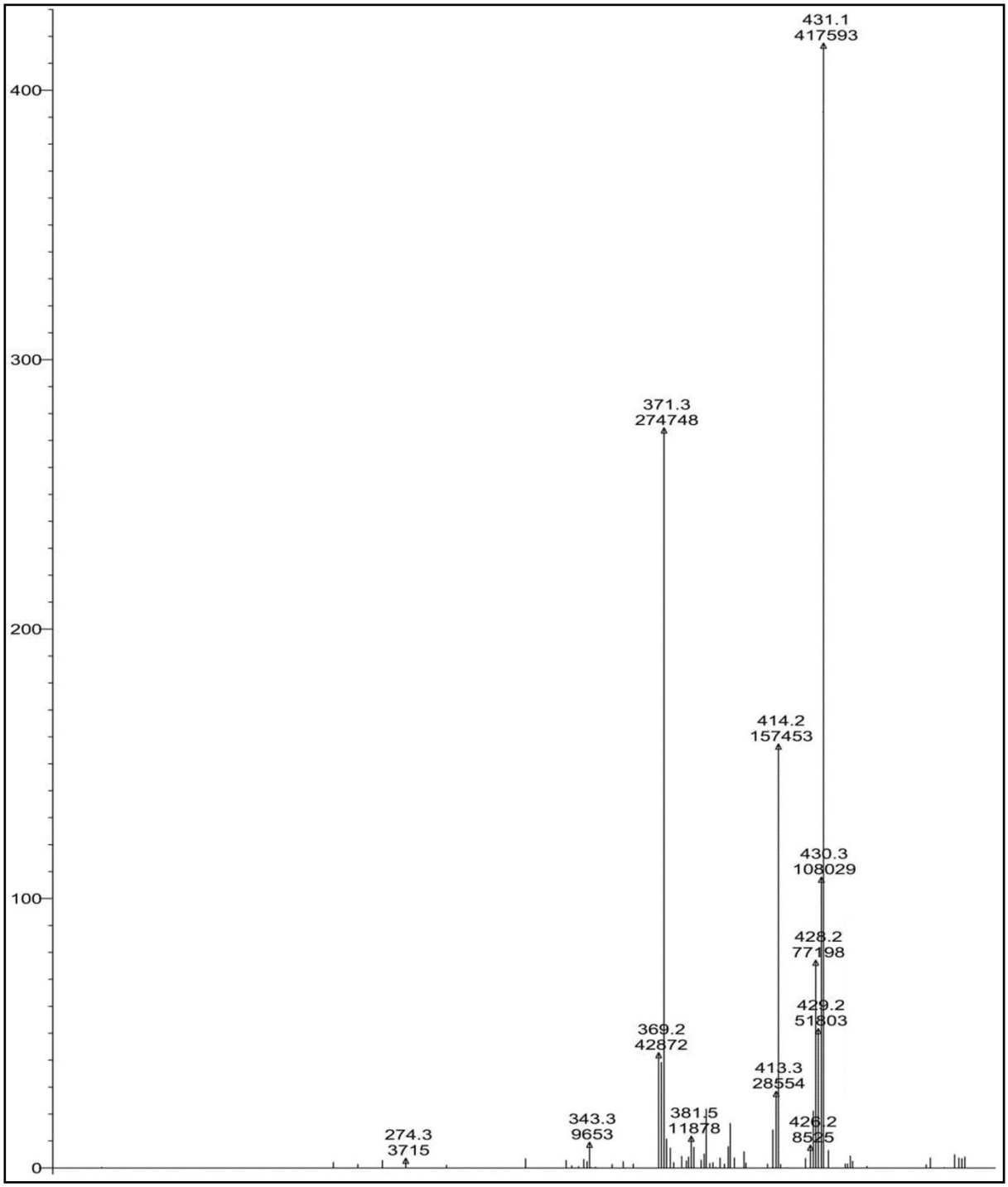

Fig. S3 LC-MS Mass spectrum of complex (**2**).

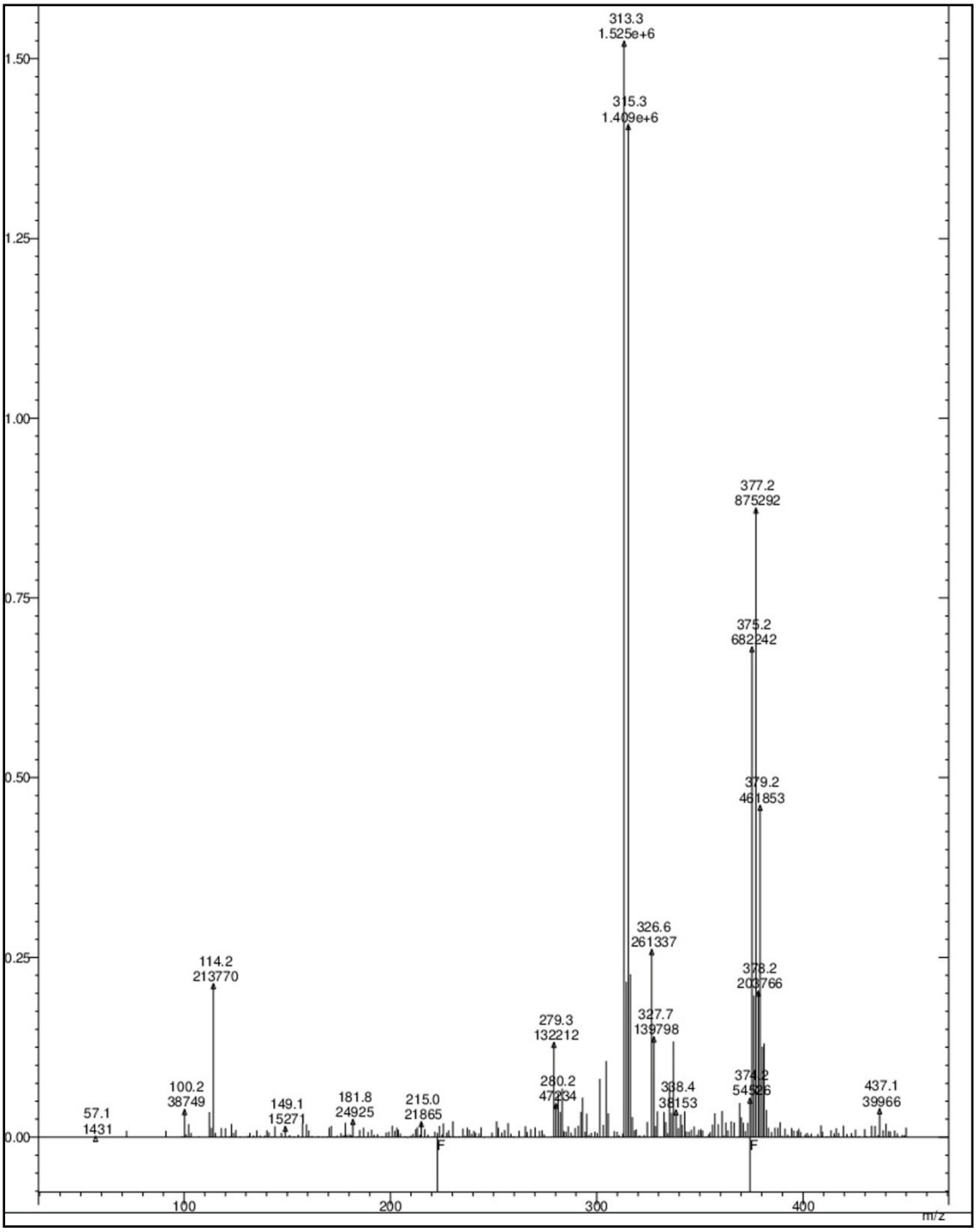

Fig. S4 LS-MS Mass spectrum of complex (**5**).

^{1}H NMR spectra

The ^{1}H NMR spectral studies were carried out in presence of $CDCl_3$ solvent. The ligand (**HL**) and its complex (**5**) show the following signals in Fig**.** S5 and listed in table S2: δ values of ligand (**HL**): aromatic protons (m, 3H) at 6.84 – 7.36 ppm; azomethine (-HC=N-) proton (s, 1H) at 8.28 ppm; morpholinic-OCH_2 protons (t, 4H) at 3.74 ppm; morpholinic-N-CH_2 (t, 4H) at 2.63 ppm; ethylene protons =N-CH_2-CH_2-N (t, 4H) in the range of 1-2.5 ppm; phenolic-OH proton (s, 1H) at 13.47 ppm.[3] Complex (**5**): aromatic protons (m, 3H) at 6.86 – 7.38 ppm; azomethine proton(-HC=N-) (s, 1H) at 8.86 ppm; morpholinic-OCH_2 (t, 4H) at 3.75 ppm; morpholinic-N-CH_2 (t, 4H) at 2.98 ppm; acetate protons (CH_3COO-) (s, 3H) at 2.029 ppm; The low intensity singlet peak at nearly 1.78 ppm which assign the lattice water protons[4] (s, 1H). The absence of singlet peak at the range of 13 ppm in the complex (**5**) indicates the loss of the –OH proton due to complexation[5] and other signals are not appreciable change in the complex (**5**).

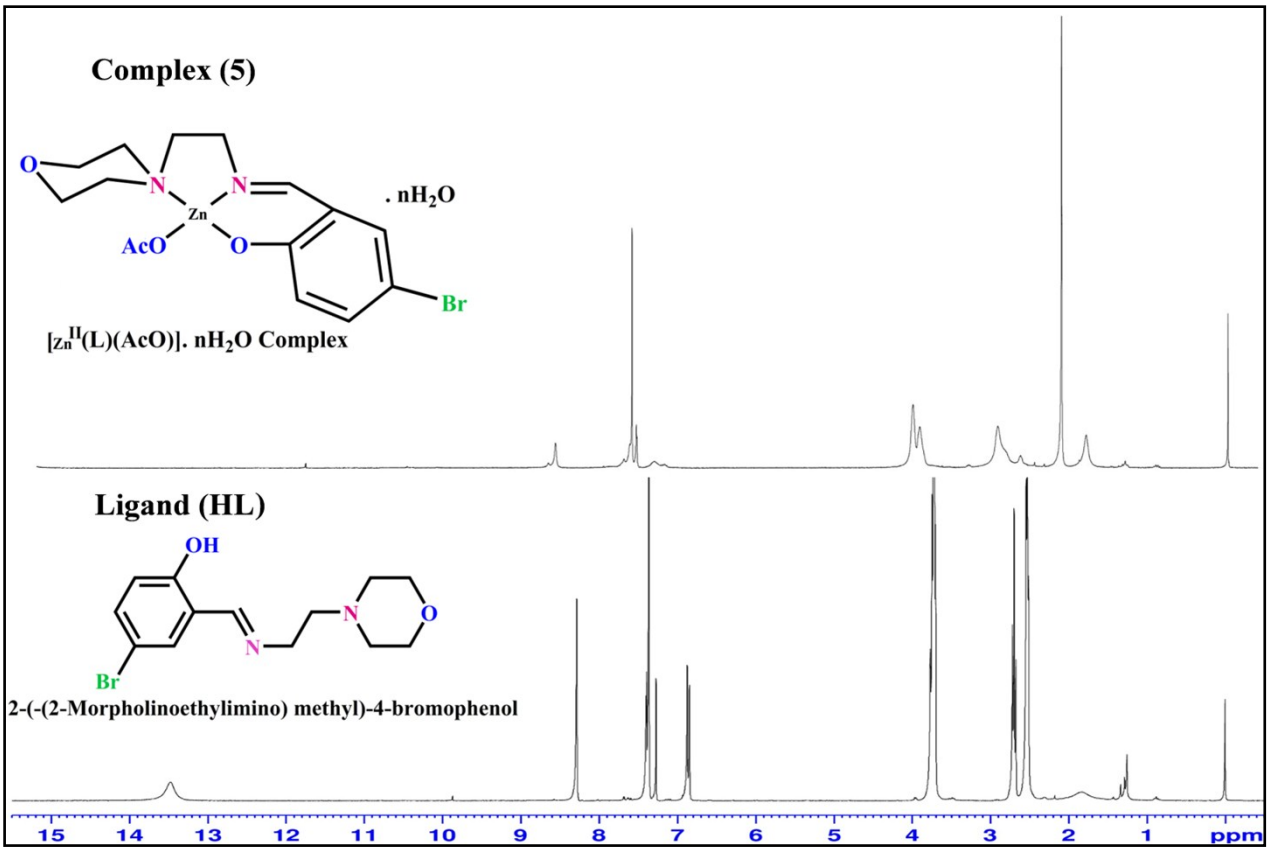

Fig. S5 ^{1}H NMR spectra of ligand (**HL**) and its complex (**5**).

Table S2 ^{1}H NMR spectral data of the ligand (**HL**) and its complex (**5**).

Compounds (in ppm)	Ar-protons (m, 3H)	HC=N- (s,1H)	Morpholino O-CH_2- (t, 4H)	Morpholino N-CH_2 (t, 4H)	Phenolic -OH (s,1H)	Acetate CH_3COO- (s,3H)	(H_2O) (s,1H)
(**HL**)	6.84 -7.36	8.28	3.74	2.63	13.47	-	-
Complex (**5**)	6.86 -7.38	8.86	3.75	2.98	-	2.029	1.78

^{13}C NMR spectrum

The ^{13}C NMR spectrum of the ligand (**HL**) was recorded by a Bruker Avance III HD Nanobay 400 MHz spectrometer operating in Fourier transform mode in the presence of $CDCl_3$ at room temperature.[6] The following signals of ligand were demonstrated in Fig**.** S6. The observed peak at 164.43 ppm was assigned iminic (azomethine) carbons. And also, various located aromatic carbons for ($\underline{C}_{Ar}$-OH), (Br-C=$\underline{C}H_{Ar}$), (Br-C-$\underline{C}H_{Ar}$), ($\underline{C}_{Ar}$-HC=N-), ($\underline{C}_{Ar}$=C-OH) and (Br-$\underline{C}_{Ar}$) were found at 160.37, 134.93, 133.34, 120.11, 119.12 and 109.94 ppm respectively. The peak of morpholinic-$\underline{C}H_2$-O-$\underline{C}H_2$ was found at 66.93 ppm. And also, the observed peaks at 56.60, 56.80 ppm are attributed to morpholinic-$\underline{C}H_2$-N-$\underline{C}H_2$ carbons. The chemical shifts for =N-CH_2-$\underline{C}H_2$-N and =N-$\underline{C}H_2$-CH_2-N groups were also obtained at 58.87 and 53.83, 53.28 respectively. Furthermore, the strong triplet peaks for $CDCl_3$ solvent was observed in the range of 76.75-77.38 ppm. The observed results are also put forwarded the locations of carbons in the ligand structure.

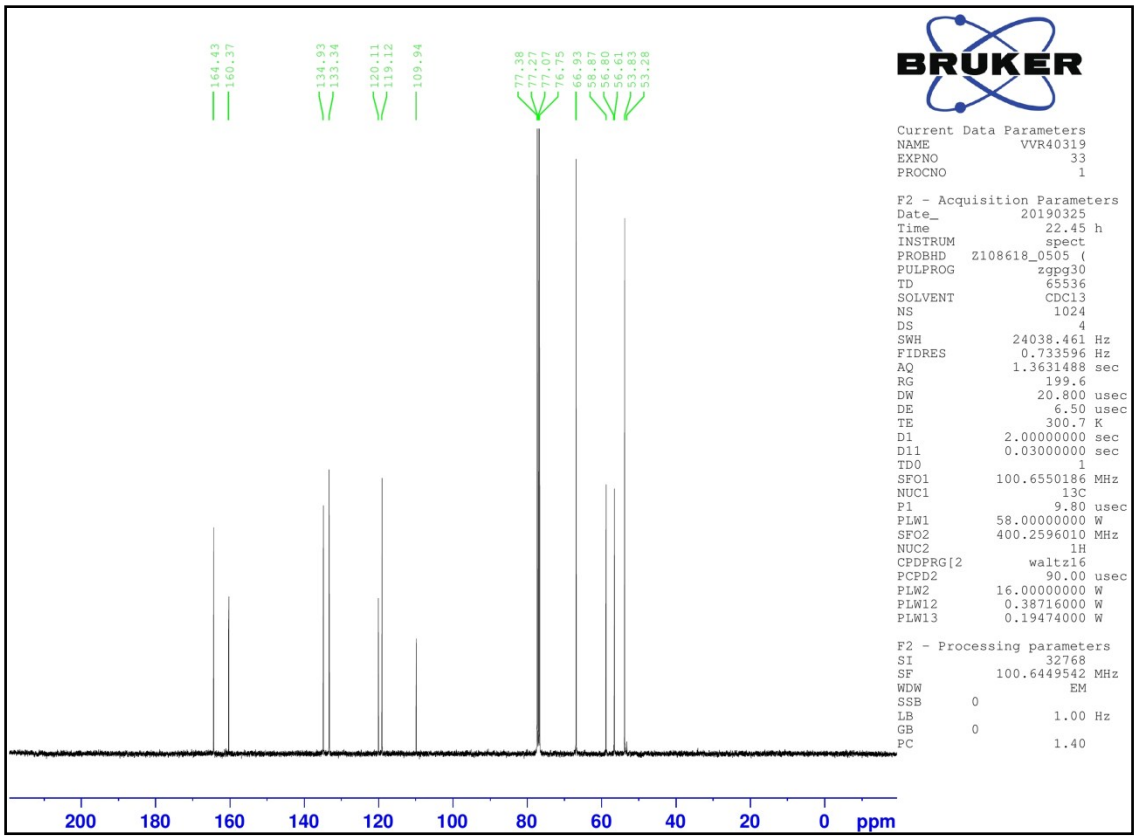

Fig. S6 ^{13}C NMR spectrum of ligand (**HL**).

Fourier Transform infrared spectra

The FTIR spectra of the complexes (**1-5**) were analysed the frequency changes of free ligand (**HL**) during the complexation and their observed results were also summarized in Table S3. IR spectrum of ligand (**HL**) exposes a strong sharp band for the azomethine (-HC=N-) group at 1639 cm^{-1} which is shifted to lower frequencies in the complexes (**1-5**) due to complexation with the central metal ion.[7] The peak of -OH group was found at 3653 cm^{-1} in the free ligand [**HL**] and the same peak is disappeared in the spectra of all complexes due to deprotonation of -OH group upon complexation[8] and also the peak due to the presence of phenolic C-O at 1273 cm^{-1} in ligand (**HL**) is shifted to higher frequencies (1295-1308 cm^{-1}) in complexes (**1-5**) indicating confirming deprotonation of the phenolic–OH on chelation[9]. Morpholinic-C-N-C bands are found at 1353 cm^{-1} in the free ligand and the bands also shifted to lower frequencies (1330 –1342 cm^{-1}) in complexes (**1-5**) due to C-N-C nitrogen coordinate

with the central metal ion. A broad band was identified (stretching) at 3423 – 3447 cm^{-1} range and another one in-plane bending weak band (rocking) was observed at 823 – 842 cm^{-1} range in the spectra of all complexes which suggest the presence of lattice water molecules in the metal complexes (**1-5**)[10]. In the spectra of complexes (**1-5**), there are found two bands for carboxylate of the acetate group which absorbs strongly in the range of 1646 – 1655 cm^{-1} ($\gamma_{asymmetry}$) and more weakly at 1388 – 1392 cm^{-1} ($\gamma_{symmetry}$) range. It further suggest that they are involved in unidentate coordination with the metal ion because of the difference values between asymmetry and symmetry stretching frequencies were greater than 200 cm^{-1} [11]. In the far IR spectra of the complexes (**1-5**), the medium bands were found in the region 452 – 465 cm^{-1} and 517 – 544 cm^{-1} which are corresponding to M-N and M-O vibrations respectively and other absorption bands have no appreciable changes in the free ligand and its complexes (**1-5**) (Table S3 and Fig. 7).

Table S3 Infrared spectral data of the ligand (**HL**) and its complexes (**1-5**).

Compounds (cm^{-1})	HC=N	Phen-C-O	Morp-C-N-C	Morp-C-O-C	C-H			Acetate CH_3COO	Ph-OH / H_2O	M-N	M-O
					Ar-C-H	Ali-C-H	Iminic H-C=N-				
(HL)	1639	1273	1353	1108 (s) 1179(as)	2978	2939	2860	---	3653	---	---
(**1**)	1627	1295	1338	1108 (s) 1179(as)	2971	2926	2868	1393 (s) 1655 (as)	3423, 830 (b)	457	544
(**2**)	1631	1306	1336	1110 (s) 1173(as)	2972	2923	2852	1393 (s) 1646 (as)	3447, 829(b)	458	521
(**3**)	1626	1303	1342	1113 (s) 1172(as)	2975	2925	2858	1394 (s) 1648 (as)	3438, 823(b)	452	517
(**4**)	1623	1306	1330	1114 (s) 1195(as)	2973	2924	2860	1393 (s) 1646 (as)	3439, 830(b)	456	534
(**5**)	1622	1308	1332	1115 (s) 1178(as)	2968	2939	2861	1388 (s) 1648 (as)	3431, 842(b)	465	542

s → symmetry, as → asymmetry, b →in-plane bending (rocking), Phen-C-O → Phenolic C-O, Morp-C-N-C → Morpholinic C-N-C, Morp-C-O-C → Morpholinic C-O-C, Ar-C-H → Aromatic C-H, Ali-C-H → Aliphatic C-H, Ph-OH → Phenolic OH.

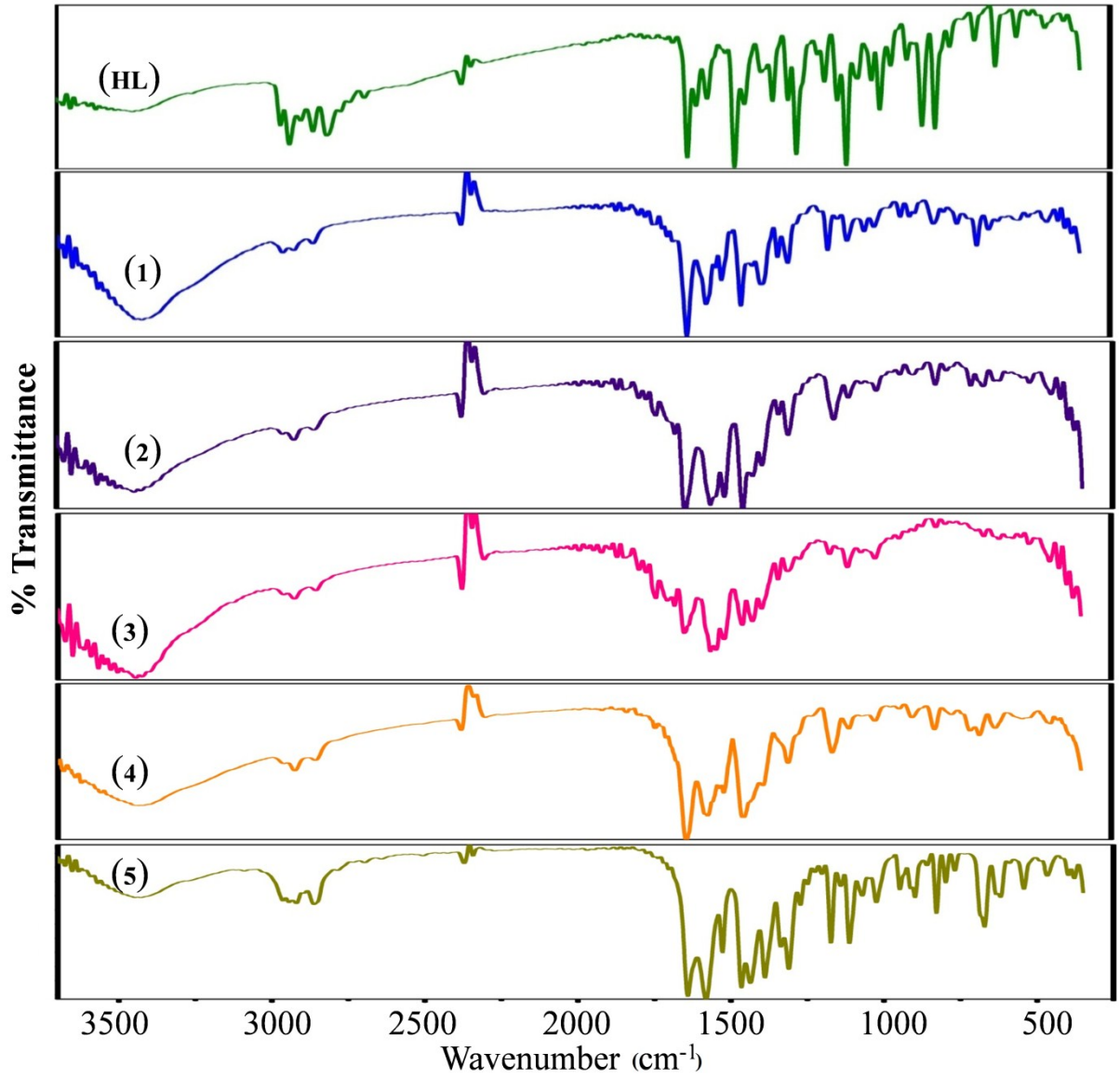

Fig. S7 FT-IR spectra of ligand (**HL**) and its complexes (**1-5**).

Electronic absorption spectra and Magnetic susceptibility

Ligand (**HL**) and its complexes (**1-5**) were recorded in methanol by electronic absorption spectrophotometer. The absorption maxima and magnetic moment values are depicted in Table S4. The free ligand (**HL**) displayed three absorption bands at 382 nm (26,178 cm^{-1}) and 297 nm (33,670 cm^{-1}), 267 nm (37,453 cm^{-1}) which are assigned n→π* and π→π* transitions respectively due to the azomethine chromophore and phenyl ring[12]. The bands in the complexes (**1-5**) are shifted to a higher wavelength due to the donation of lone pair electron in a sp^2-hybridized orbital of the imino nitrogen atom of the ligand (**HL**) to the metal centre. In general, Copper(II) complexes show only one broad band in the visible region. However, It is difficult to resolve it into three bands which is due to the fact that the four d-orbitals, d_z^2, d_{xy}, d_{xz} and d_{yz} lie close together[13]. The present copper complex (**1**) has exhibited two d–d bands, in which one broad band centered at 643 nm (15,552 cm^{-1}), which can be assigned to the $^2B_{1g}\rightarrow{}^2B_{2g}$ transitions due to John-Teller distortion and another one found at 405 nm (24,691 cm^{-1}) which can be assigned to $^2B_{1g}\rightarrow{}^2E_g$ transition and also another two bands appeared in the region of 357 nm (28,011 cm^{-1}), 283 (35,335) which are indicaed to intra-ligand charge transfer and π→π* transitions respectively. Ray-Sen (1948) and Condon-Shortley (1951) suggested that Cu(I1) square planar and tetrahedral configurations must have magnetic moments nearly about 1.73 B.M and 2.2 B.M respectively.[14] The observed magnetic susceptibility value (μ_{eff}) of the complex (**1**) was 1.85 B.M which is slightly higher than the spin-only value (1.73 B.M) for one unpaired electron[15-17] and complex (**1**) has not revealed any d–d electronic absorption bands in the region of 1000–1200 nm.[18,19] it is also a strong evidence for square planar geometry. Furthermore, the structures of four-coordinated Cu(I) and Cu(II) species may occur intermediate state between square planar and tetrahedral geometries in some cases. It also attributes that the oxidation state plays a leading role in the

geometry formed d^{10} Cu(I) complexes which favors to four-coordinated tetrahedral geometries due to the lack of ligand field stabilization energy and d^9 copper(II) configuration prefers to four-coordinated square planar geometries. However, the splitting is strong evidence of the stereochemical unequivalency of aromatic and azomethine groups in the present complex (**1**), which suggests that both exhibits square planar geometry distorted towards tetrahedral.[20] Complex (**2**) reveals two absorption d–d bands at 664 nm (15,060 cm^{-1}) and 466 nm (21,459 cm^{-1}) which are assigned to $^4A_{2g} \rightarrow {}^4T_{1g}(F)$ and $^4A_{2g} \rightarrow {}^4T_{1g}(P)$ transitions respectively and another two bands 351nm (28,490 cm^{-1}), 282 nm (35,461 cm^{-1}) are due to the intra-ligand charge transfer and $\pi \rightarrow \pi^*$ transitions. The μ_{eff} value of the complex (**2**) was observed at 4.22 B.M which was higher than spin-only moment value (3.88 B.M) due to mixing of the ground state with a comparatively low lying excited state. The magnetic moment result and the blue colour of the cobalt(II) complex are strongly recommended to tetrahedral geometry.[21, 22] The absorption spectrum of the complex (**4**) shows two d-d bands at 691nm (14,471 cm^{-1}) and 492 (20,325 cm^{-1}) which are assigned as $^1A_{1g}(D) \rightarrow {}^1B_{1g}(G)$ and $^1A_{1g}(D) \rightarrow {}^1A_{2g}(G)$ transitions and other two bands 382 (26,178 cm^{-1}), 273 (36,630 cm^{-1}) are due to the intra-ligand charge and $\pi \rightarrow \pi^*$ transfer transitions respectively and also the complex (**4**) is diamagnetic behaviour due to the effective magnetic moment value (μ_{eff}) is zero BM.[23, 24] which is strongly proposed that Nickel(II) complex has attained square planar geometry due to stronger stabilization coordination sphere as compared to copper complex(**1**).[25] Complexes (**3**) and (**5**) have no absorption bands in the visible domain which is in good agreement with the electronic structure of the central metallic ion with d^5 and d^{10} electronic configurations respectively. The prediction of geometry of these complexes by crystal field theory is difficult task due to absence of d-d transitions. In addition, two absorption bands at 396 nm (25,252 cm^{-1}), 380 nm (26,315 cm^{-1}) for INCT transitions and 272 nm (36,764 cm^{-1}) for $\pi \rightarrow \pi^*$ transitions were observed in the complex (**3**) and also the observed effective

magnetic moment value (μ_{eff}) was 1.77 B.M which is highly recommended to square planar geometry.[26,27]. Complex (**5**) showed two absorption bands at 378 nm (26,455 cm^{-1}), 355 nm (28,169 cm^{-1}) for INCT transitions and 243 nm (41,152 cm^{-1}) for $\pi \rightarrow \pi^*$ transitions and there is no ligand field stabilization effect in Zn^{2+} ions because of its complete d shell and diamagnetic behaviour. The results are proposed that complex (**5**) possess tetrahedral geometry around the central metal(II) ion.[28] (Table.S4 and Fig.S8).

Table S4 Electronic spectral data and magnetic susceptibility values of the synthesized compounds.

Compounds	Band Position λ_{max} nm (γ-cm^{-1})	Assignment	μ_{eff} (B.M)	Geometry
(**HL**)	382 (26,178)	$n \rightarrow \pi^*$	--	--
	297 (33,670)	$\pi \rightarrow \pi^*$		
	267 (37,453)	$\pi \rightarrow \pi^*$		
(**1**)	643 (15,552)	$^2B_{1g} \rightarrow {}^2B_{2g}$	1.85	Distorted Square planar
	405 (24,691)	$^2B_{1g} \rightarrow {}^2E_g$		
	357 (28,011)	INCT		
	283 (35,335)	$\pi \rightarrow \pi^*$		
(**2**)	664 (15,060)	$^4A_{2g} \rightarrow {}^4T_{1g}(F)$	4.22	Tetrahedral
	466 (21,459)	$^4A_{2g} \rightarrow {}^4T_{1g}(P)$		
	351 (28,490)	INCT		
	282 (35,461)	$\pi \rightarrow \pi^*$		
(**3**)	396 (25,252)	INCT	1.77	Square planar
	380 (26,315)	INCT		
	272 (36,764)	$\pi \rightarrow \pi^*$		
(**4**)	691 (14,471)	$^1A_{1g}(D) \rightarrow {}^1B_{1g}$ (G)	DM	Square planar
	492 (20,325)	$^1A_{1g}(D) \rightarrow {}^1A_{2g}$ (G)		
	382 (26,178)	INCT		
	273 (36,630)	$\pi \rightarrow \pi^*$		
(**5**)	378 (26,455)	INCT	DM	Tetrahedral
	355 (28,169)	INCT		
	243 (41,152)	$\pi \rightarrow \pi^*$		

INCT→ Inraligand charge transfer, μ_{eff} → Effective magnetic moment, B.M→ Bohr magnetons, DM →diamagnetic nature.

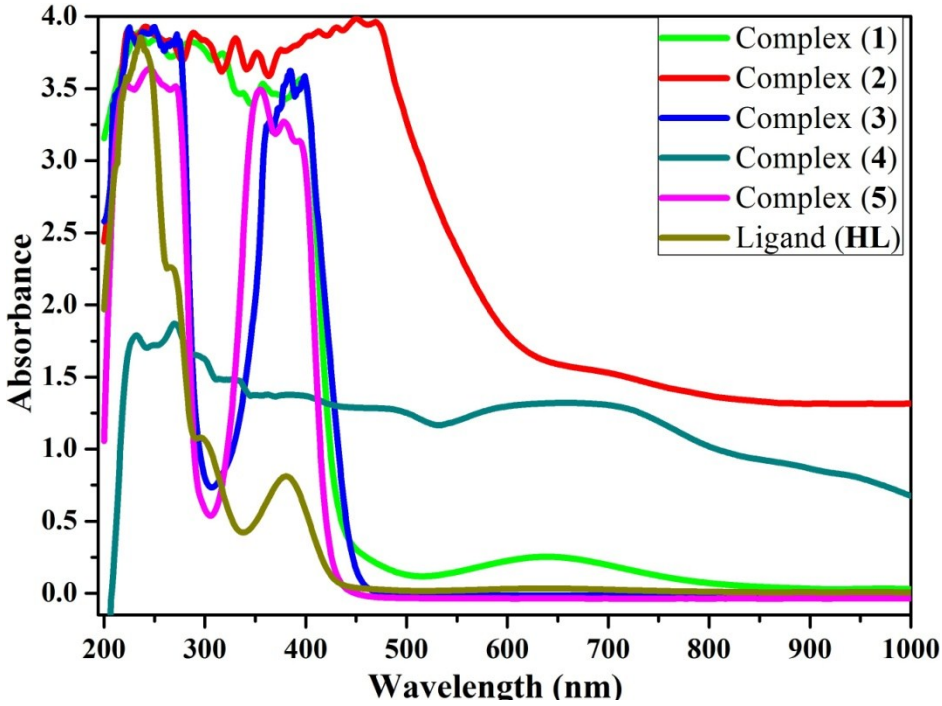

Fig. S8 Electronic spectra of ligand (**HL**) and its complexes (**1-5**).

EPR spectra

The solid state EPR spectra of copper complex (**1**) was recorded in the X-band region at liquid nitrogen temperature (77 K) under 9.10 GHz microwave field modulation using tetracyanoethylene (g_e = 2.00277). Figure S9 shows the EPR spectrum of complex (**1**) and the data are summarized in Table S5. The complex (**1**) is exhibited anisotropic pattern with well-resolved hyperfine lines at 77 K. The spin hamiltonian parameters were calculated by Kivelson's method.[29] In the distorted square planar complexes, if the unpaired electron lies in the $d_{x^2-y^2}$ orbital ($^2B_{1g}$) as the ground state it leads to the following order $g_{\|} > g_{\perp} > g_e$. If the unpaired electron lies in the dz^2 orbital ($^2A_{1g}$) as the ground state, it attains the order $g_{\perp} > g_{\|} > g_e$. The observed g-values are found in the following order $g_{\|}$ (2.24) > $g_{\perp}$ (2.03) > g_e (2.00277). It further confirms the covalent character of the M-L bond due to $g_{\|}$ values are less than 2.3 [30] and the observed g_{eff} (1.42) value from the equation (**4**) was further supportive due to it is less than 2.00277.[31] The measured hyperfine constant parameters were in the

consequent order $A_{\|}$ (165 G) > A_{av} (78.33 G) > $A_{\perp}$ (35 G). It is clear that the EPR parameters of the complex (**1**) agree with the related system which suggests that the complex has square planar geometry with axially symmetrical.[32] The values were obtained from the following equations (1-6). The observed geometric parameter value of G (7.55) was greater than 4 suggesting that there is no interaction between Cu-Cu centers in the solid state complex (**1**) and the absence of half field signal at 1600G corresponding to the $\Delta Ms = \pm 2$ transition rules out a Cu-Cu interaction.[33, 34] The values of molecular orbital coefficient parameters α^2, β^2 and γ^2 were measured from Kivelson and Neimann formulae (7-9). In-plane σ-bonding parameter $\alpha^2 = 1.0$ indicates the pure ionic character. Whereas, $\alpha^2 = 0.5$ indicates the pure covalent bonding. The obtained value of α^2 was 0.74 which indicates that the complex has covalent character and also the observed $\beta^2 = 0.76$ (in-plane π-bonding) and $\gamma^2 = 0.41$ (out-plane π-bonding) values were less than 1.0 which attributes that π-bonding is completely covalent character.[35] According to Hathaway and Tomlinson concept,[36, 37] if the orbital reduction factors $K_{\|}$ and $K_{\perp}$ are equal, it shows the pure σ-bonding. In general, if the value of $K_{\|}$ is less than $K_{\perp}$, it represents in-plane π-bonding and if the $K_{\|}$ value is greater than $K_{\perp}$, it also assigns out-of-plane π–bonding. However, the observed value of $K_{\|}$ (0.56) was greater than $K_{\perp}$ (0.30) for the complex (**1**), which indicates the presence of out-plane π-bonding in metal ligand π–bonding and the values are also calculated from the equations (10-11). The Co-factor value of degree of geometrical distortion ($f_{\|}$ = 135.80 cm^{-1}) was measured from equations (12).[38, 39] the result strongly attributes the square planar geometry around the Cu(II) ion. And also, Fermi contact hyperfine interaction term (K_{fermi} = 0.29) value was calculated from the equations (13-15) with help of dipolar term (P) (Table S4) which is further supportive to measure the polarization produced by the uneven distribution of d-electron density on the inner core s-electron. The hyperfine interaction value $K \geq 1$ denotes ionic environment and $K < 1$ also assigns covalent environment, the observed value of K (0.39) was less than 1.0 which

designates the greater covalent character. The obtained all results propose that complex (**1**) has distorted square planar geometry which good agree with electronic absorption results.

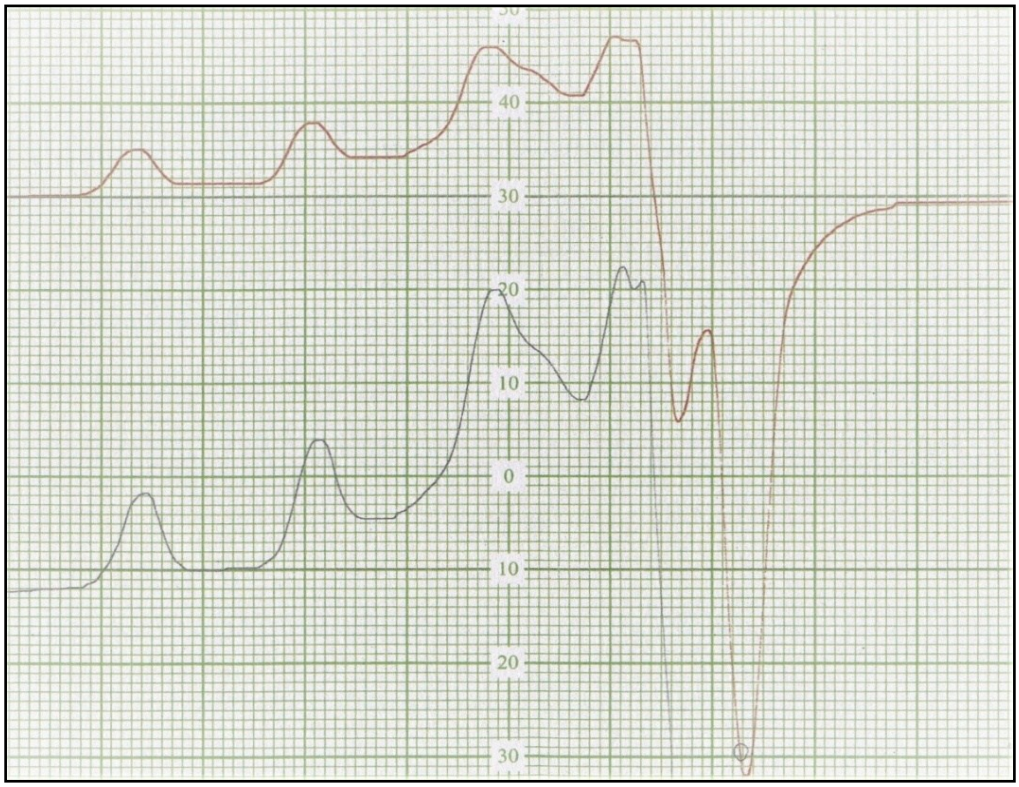

Fig. **S9.** The EPR spectra of complex (**1**) at liquid nitrogen temperature (77 K).

Table S5 The spin Hamiltonian parameters of complex (**1**) at 77K.

	g tensor				**Hyperfine constant × 10^{-4} (cm^{-1})**				
	$g_{\parallel}$	$g_{\perp}$	g_{av}	g_{eff}	$A_{\parallel}$	$A_{\perp}$	A_{av}		
	2.24	2.03	2.08	1.42	165	35	78.33		
Complex (**1**)	**Bonding Parameters**								
	G	$f_{\parallel}$ (cm^{-1})	α^2	β^2	γ^2	$K_{\parallel}^2$	$K_{\perp}^2$	K	K_{fermi}	μ_{eff}
	7.55	135.80	0.74	0.76	0.41	0.56	0.30	0.39	0.29	1.80

g_e = 2.00277, Microwave frequency (γ') = 9.114 × 10^9cycle/sec, 1G = 10^{-4} cm^{-1}, E_{d-d} = 15,552 cm^{-1}, one-electron spin orbit coupling constant of free Cu(II) ion λ_0 = - 828 cm^{-1}; (**1**). $g_{\perp} = \frac{(3g_{av} - g_{||})}{2}$; (**2**).

$K_{\perp} = \frac{(3A_{av} - A_{||})}{2}$; (**3**). $g_{av} = \frac{(g_{||} + 2g_{\perp})}{3}$; (**4**). $g_{eff} = \frac{(g_{||} + g_{\perp})}{3}$; (**5**). $A_{av} = \frac{(A_{||} + 2A_{\perp})}{3}$;

(**6**). $G = \frac{(g_{||} - 2.00277)}{(g_{\perp} - 2.00277)}$; (**7**). $\alpha^2 = \frac{A_{||}}{P} + (g_{||} - 2.00277) + \frac{3}{7}(g_{\perp} - 2.00277) + 0.04$; (**8**).

$\beta^2 = (g_{||} - 2.00277)(\frac{E_{d-d}}{-8\lambda_0 a^2})$; (**9**). $\gamma^2 = (g_{\perp} - 2.00277)(\frac{E_{d-d}}{-2\lambda_0 a^2})$; (**10**).

$K_{||}^2 = (g_{||} - 2.00277)(\frac{E_{d-d}}{-8\lambda_0})$; (**11**). $K_{\perp}^2 = (g_{\perp} - 2.00277)(\frac{E_{d-d}}{-2\lambda_0})$; (**12**). $f_{||} = g_{||} / A_{||}$; (**13**).

$K = \frac{(K_{||}^2 + 2K_{\perp}^2)}{3}$; (**14**). $K_{fermi} = \frac{A_{av}}{P\beta^2} + \frac{(g_{av} - 2.00277)}{\beta^2}$; (**15**). Free ion dipolar term $P = 2\,\Upsilon_{Cu}\,\beta_0 B_N\,(\gamma^{-3}) = 0.036$ cm^{-1}; (**16**). $\mu_{eff} = g_{av}\,[S(S+1)]^{1/2}$; μ_{exp} = 1.85 B.M, Magnetic susceptibility (μ_{eff}); Υ_{Cu} = magnetic moment value for copper, β_0 = Bohr Magneton, B_N = Nuclear Magneton, γ = the distance from the central nucleus to the electron; Molecular orbital coefficient parameters α^2, β^2 and γ^2 , Co-factor ($f_{||}$) value of degree of geometrical distortion; Ionic environment (K, K_{fermi}).

Thermogravimetric analysis (TGA)

TGA is an efficient and essential dynamic technique to assess the quantitative of weight changes with respect to temperature and to explore the thermal stability and composition of complexes[40] and also it is very supportive for investigating the probability of attachment of solvent molecules (H_2O) towards the central atom as a crystal or in a coordinate form / lattice form. Thermogram of the complexes (**1-5**) has been recorded in the temperature range from 40 °C to 750 °C (Fig. S10 & 11). The stages of decomposition, temperature range, decomposition products, the observed mass loss and calculated mass loss percentages of complexes (**1-5**) are summarized in Table S6. Complexes (**1-5**) were thermally decomposed in three steps. In the first step endothermic process, the observed weight losses of decomposition of $[M^{II}(L)AcO].nH_2O$ complexes (**1-5**) were found as follows 04.12 % (03.97 %) (**1**), 14.30 % (14.33 %) (**2**), 15.04 % (14.45 %) (**3**), 14.85 % (14.34 %) (**4**) and 8.05 % (07.61 %) at 120, 103, 98, 98 and 120 °C respectively which corresponds to the loss of hydrated lattice water molecules.[41, 42] The observed weight losses in the second degradation stages were declared that the 31.20 % (31.14 %) (**1**), 28.10 % (28.07 %) (**2**), 28.36 % (28.30 %) (**3**), 28.12 % (28.09 %) (**4**) and 29.86 % (29.83 %) (**5**) for the elimination of the morpholine ($C_7H_{13}N_2O$) moiety in the temperature range of 120–420 °C. The obtained weight losses in the third degradation stage were indicated that the 47.22 % (47.27 %) (**1**), 42.70 % (42.61 %) (**2**), 43.05 % (42.95 %) (**3**), 42.74 % (42.63 %) (**4**) and 45.35 % (45.28 %) (**5**) for removal of the acetate ($C_2H_3O_2$) and aromatic (C_6H_3Br) moieties in the temperature range of 420–750 °C.

The final percentage of remaining products was found 17.60 % (17.55 %) (**1**), 15.06 (14.87) (**2**), 14.88 (14.24) (**3**), 15.02 (14.88) (**4**) and 17.82 (17.21) (**5**) in this complexes (**1-5**) respectively which disclose the formation of MO residue.[43] The overall thermal degradation steps of complexes (**1-5**) are possible as in the following flow chart. Based on the above results, the proposed structures of complexes (**1-5**) have been shown in Scheme 1.

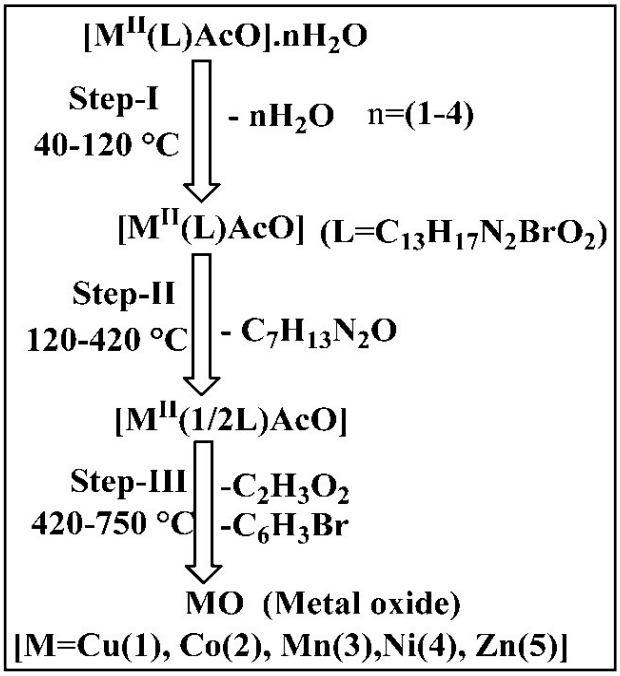

Fig. S10. The various stages for thermal decomposition of metal complexes (**1-5**) at temperature range of 40 -750 °C.

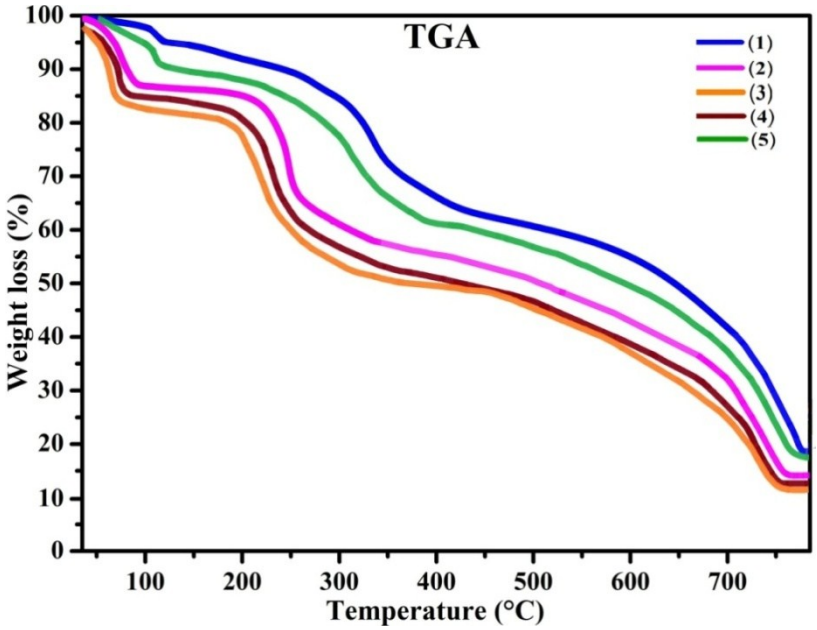

Fig. S11. TG plots of complexes (**1-5**) recorded under nitrogen atmosphere between the temperature range 40 and 750 °C at a heating rate of 20 °C/min.

Table S6 Thermal analysis of complexes (**1-5**) by TGA method.

Complexes	M.W	Step	Temperature range (°C)	% Weight loss [found (calcd)]	Assignment
(**1**) [Cu^{II}(L) AcO].H_2O ($C_{15}H_{21}N_2BrO_5$)Cu	452.75	I	40–120	04.12 (03.97)	H_2O
		II	120–420	31.20 (31.14)	$C_7H_{13}N_2O$
		III	420–750	47.22 (47.27)	$C_2H_3O_2$, C_6H_3Br
		Residue	>750	17.60 (17.55)	CuO
(**2**) [Co^{II}(L) AcO].$4H_2O$ ($C_{15}H_{28}N_2BrO_8$)Co	502.14	I	40–103	14.30 (14.33)	$4H_2O$
		II	120–420	28.10 (28.07)	$C_7H_{13}N_2O$
		III	420–750	42.70 (42.61)	$C_2H_3O_2$, C_6H_3Br
		Residue	>750	15.06 (14.87)	CoO
(**3**)[Mn^{II}(L) AcO].$4H_2O$ ($C_{15}H_{28}N_2BrO_8$)Mn	498.15	I	40–98	15.04 (14.45)	$4H_2O$
		II	120–420	28.36 (28.30)	$C_7H_{13}N_2O$
		III	420–750	43.05 (42.95)	$C_2H_3O_2$, C_6H_3Br
		Residue	>750	14.88 (14.24)	MnO
(**4**) [Ni^{II}(L) AcO].$4H_2O$ ($C_{15}H_{28}N_2BrO_8$)Ni	501.91	I	40–98	14.85 (14.34)	$4H_2O$
		II	120–420	28.12 (28.09)	$C_7H_{13}N_2O$
		III	420–750	42.74 (42.63)	$C_2H_3O_2$,

		Residue	>750	15.02 (14.88)	C_6H_3Br NiO
(**5**) $[Zn^{II}(L)\ AcO].2H_2O$ $(C_{15}H_{23}N_2BrO_6)Zn$	472.58	I	40–110	8.05 (07.61)	$2H_2O$
		II	120–420	29.86 (29.83)	$C_7H_{13}N_2O$
		III	420–750	45.35 (45.28)	$C_2H_3O_2$, C_6H_3Br
		Residue	>750	17.82 (17.21)	ZnO

References

1. V. M. Manikandamathavan, T. Weyhermüller, R. P. Parameswari, M. Sathishkumar, V. Subramanian and B. U. Nair, *Dalton Trans.*, 2014, **43**, 3018–13031.
2. F. Sama, A. K. Dhara, M. N. Akhtar, Y. C. Chen, M. L. Tong, I. A. Ansari, M. Raizada, M. Ahmad, M. Shahid and Z. A. Siddiqi, *Dalton Trans.*, 2017, **46**, 9801–9823.
3. R. M. Silverstein, F. X. Webster, D. J Kiemle and D. L. Bryce, *Spectrometric Identification of Organic Compounds*. *8th edition, New York, John Wiley and Sons*, 2014, 1–464. ISBN: 978-0-470-61637-6.
4. E. Tas, M. Aslanoglu, A. Kilic, O. Kaplana and H. Temel, *J. Chem. Res.*, 2006, **2006**, 242–245.

5. M. Asadi, N. Savaripoor, Z. Asadi, M. H. Ghatee, F. Moosavi, R. Yousefi and M. Jamshidi, *Spect. Chim. Acta Part A: Mol and Biomol. Spect.*, 2013, **101**, 394–399.

6. S. B. Jimenez-Pulido, F. M, Linares-Ordonez, M. N, Moreno-Carretero and M. Quiros-Olozabal, *Inorg. Chem.,* 2008, **47**, 1096–1106.

7. E. S. Aazam, A. F. EL Husseiny and H. M. Al-Amri, *Arab. J. Chem*., 2012, **5**, 45–53.

8. N. Raman, J. D. Raja and A. Sakthivel, *Russ. J. Coord. Chem*., 2008, **34,** 400–406.

9. Y. Li, Z. Y. Yang, Z. C. Liao, Z. C. Han and Z. C. Liu, *Inorg. Chem. Comm*., 2010, **13**, 1213–1216.

10. M. S. Masoud, M. F. Amira, A. M. Ramadan and G. M. El-Ashry, *Spect. Chim. Acta Part A: Mol and Biomol. Spect.*, 2008, **69**, 230–238.

11. S. Chandra and L. K. Gupta, *Spect. Chim. Acta Part A: Mol and Biomol. Spect.*, 2005, **61**, 269–275.

12. M. Shakir, A. Abbasi, M. Azam and A. U. Khan, *Spect. Chim. Acta Part A: Mol and Biomol. Spect.*, 2011, **79**, 1866–1875.

13. Y. Nishida and S. Kida, *Coord. Chem. Rev.,* 1979, **27**, 275–298.

14. K. Ito and T. Ito, *Australian. J. Chem*., 1958, **11**, 406–414.

15. S. Tabassum, A. Bashar, F. Arjmand and K. S. Siddiqi, *Synth and React in Inorg and Met-Org. Chem.*, 1997, **27**, 487–503.

16. A. D. Kulkarni, S. A. Patil, V. H. Naik and P. S. Badami, *Med. Chem Res.*, 201, **20**, 346–354.

17. O. Schlager, K. Wieghardt, A. Rufińska and B. Nuber, *Dalton Trans*., 1996, **8**, 1659–1668.

18. S. Konstantinovic, B. Radovanovic, Z. Cakic and V. Vasic, *J. Serb. Chem. Soc.*, 2003, **68**, 641–647.

19. L. Yang, D. R. Powell and R. P. Houser, *Dalton. Trans*., 2007, **9**, 955–964.

20. N. Raman, R. Jeyamurugan, A. Sakthivel and L. Mitu, *Spect. Chim. Acta Part A: Mol and Biomol. Spect.*, 2010, **75**, 88–97.

21. S. Konstantinovic, B. Radovanovic, Z. Cakic and V. Vasic, *J. Serb. Chem. Soc*., 2003, **68**, 641–647.

22. F. A. Cotton and G. Wilkinson, *Adv Inorg Chem*, Wiley, New York, 1989.

23. A. H. Kianfar, L. Keramat, M. Dostani, M. Shamsipur, M. Roushani and F. Nikpour *Spect. Chim. Acta Part A: Mol and Biomol. Spect.*, 2010, **77**, 424–429.

24. C. Natarajan, P. Tharmaraj and R. Murugesan, *J. Coord. Chem.*, 1992, **26**, 205–213.

25. M. Barwiolek, E. Szlyk, A. Surdykowski and A. Wojtczak, *Dalton. Trans*., 2013, **42**, 11476–11488.

26. A. A. A. Emara, A. M. Ali, A. F. El-Asmy and E.S. M. Ragab, *J. Saudi. Chem. Soc.,* 2014, **18**, 762–773.

27. V. P. Singh, S. Singh and A. Katiyar, *J. Enzyme Inhibit. Med. Chem*., 2009, **24**, 577–588.

28. J. Sandström, M. Dahlén and C. Frisell, *Acta. Chemi.Scandinavica*., 1962, **16**, 2395–2405.

29. D. Kivelson and R. Neiman, *J. Chem. Phy*., 1961, **35**, 149–155.

30. V. Venkateswaran, *Networks*., 1989, **19**, 173–173.

31. A. Syamal, *J. Chem. Edu*., **62**, 143. doi: 10.1021/ed062p143.

32. R. K. Ray and G. B. Kauffman, *Inorg. Chim. Acta.*, 1990, **173**, 207–214.

33. B. J. Hathaway and D. E. Billing, *Coord. Chem. Rev*, 1970, **5**, 143–207.

34. A. L. Sharma, I. O. Singh, M. A. Singh, H. R. Singh, R. M. Kadam, M. K. Bhide and M. D. Sastry, *Trans. Met. Chem*., 2001, **26**, 532–537.

35. Y. Z. Tang, G. X. Wang, Q. Ye, R. G. Xiong and R. X. Yuan, *Crystal Growth & Design.*, 2007, **7**, 2382–2386.

36. B. J. Hathaway, G. Wilkinson, R. D. Gillard and J. A. McCleverty, *Comprehen. Coord. chem*. *U K, Pergamon Oxford press.*,1987.

37. B. J. Hathaway and A. A. G. Tomlinson, Coord. Chem. Rev., 1970, **5**, 1–43.

38. R. P. John, A. Sreekanth, V. Rajakannan, T. A. Ajith and M. R. P. Kurup, *Polyhedron*., 2004, **23,** 2549–2559.

39. E. B. Seena and M. R. P. Kurup, *Polyhedron*., 2007, **26**, 829–836.

40. W. Gurnule, P. Rahangdale, L. Paliwal and R. Kharat, *Reactive and Functional Polymers*., 2003, **55**, 255–265.

41. I. Łakomska, M. Barwiołek, A. Wojtczak and E. Szłyk, *Polyhedron.*, 2007, **26**, 5349–5354.

42. M. A. El-Kemary, H. S. El-Gezawy, H. Y. El-Baradie and R. M. Issa, *Spect. Chim. Acta Part A: Mol and Biomol. Spect.*, 2002, **58**, 493–500.

43. A. S. Aswar and N. S. Bhave, *Thermochimica Acta.*, 1990, **157**, 233–240.

Tables:

Table S7 Relative specific viscosity Vs [Complex] / [DNA].

Compounds	Binding ratio (R) = [Complex] / [DNA]				
	0.2	0.4	0.6	0.8	1.0
	Relative specific viscosity $(\eta/\eta_0)^{1/3}$				
EB (Control)	1.01	1.35	1.63	1.82	1.99
Complex (**1**)	0.94	1.18	1.32	1.45	1.71
Complex (**2**)	0.86	0.97	1.05	1.12	1.64
Complex (**3**)	0.71	0.74	0.82	0.88	1.21
Complex (**4**)	0.78	0.85	0.92	1.02	1.32
Complex (**5**)	0.83	0.88	0.95	1.05	1.25
Ligand (**HL**)	0.70	0.76	0.86	0.96	1.10

η → Specific viscosity of DNA in the presence complex,
η_0 → Specific viscosity of DNA alone

Table S8a IC_{50} values of DPPH radical scavenging assay at 517 nm.

[Complex] μM	% Inhibition (IC_{50})						
	(**1**)	(**2**)	(**3**)	(**4**)	(**5**)	(**HL**)	Ascorbic acid
40	18.46	15.27	11.12	12.36	10.34	10.11	41.63
80	31.89	31.90	20.95	23.09	18.28	17.42	53.74
120	36.58	47.80	24.77	30.22	26.73	28.64	58.95
160	52.36	53.60	34.93	38.33	40.21	36.52	70.86
200	65.45	64.16	45.11	50.43	52.43	40.33	82.75
240	74.89	70.11	53.52	55.63	61.15	50.64	82.75

Table S8b IC_{50} values of Hydroxyl radical scavenging assay at 230 nm.

[Complex] μM	% Inhibition (IC_{50})						
	(**1**)	(**2**)	(**3**)	(**4**)	(**5**)	(**HL**)	Ascorbic acid
40	08.28	07.82	06.74	08.17	08.05	07.95	20.73
80	16.57	15.63	14.66	15.78	16.10	15.03	36.46
120	33.44	31.25	30.19	32.82	32.53	29.87	47.87
160	39.18	38.36	36.76	38.82	37.45	35.74	59.65
200	47.16	45.73	44.73	46.76	45.86	43.52	65.64
240	56.07	55.66	52.21	55.40	54.60	51.78	78.83

Table S8c IC_{50} values of Superoxide scavenging assay at 590 nm.

[Complex]	% Inhibition (IC_{50})						
μM	(**1**)	(2)	(**3**)	(**4**)	(**5**)	(**HL**)	Ascorbic acid
40	05.42	04.03	07.15	04.29	06.31	05.51	29.64
80	16.30	13.00	11.51	14.58	12.30	12.18	41.72
120	33.22	26.50	19.63	24.06	22.28	20.45	55.63
160	49.23	44.80	29.31	41.42	31.77	34.73	66.75
200	61.68	58.27	39.29	52.53	43.18	41.13	72.55
240	71.60	65.34	53.84	60.57	55.53	50.62	84.85

Table S8d IC_{50} values of Nitric oxide scavenging assay at 546 nm.

[Complex]	% Inhibition (IC_{50})						
μM	(**1**)	(**2**)	(**3**)	(**4**)	(**5**)	(**HL**)	Ascorbic acid
40	14.28	12.78	10.84	15.35	12.63	10.72	28.55
80	22.59	20.93	16.63	19.77	17.24	15.56	35.75
120	29.30	27.65	19.42	25.81	21.87	18.55	43.65
160	35.25	34.42	29.43	35.75	37.78	28.73	52.68
200	43.55	40.83	39.86	42.88	41.76	39.38	63.72
240	64.16	58.54	51.98	56.53	52.35	50.20	72.73

Table S8e IC_{50} values of Ferric reducing power scavenging assay at 700 nm.

[Complex]	% Inhibition (IC_{50})						
μM	(**1**)	(**2**)	(**3**)	(**4**)	(**5**)	(**HL**)	Ascorbic acid
40	11.24	10.64	09.74	11.02	10.75	10.34	22.68
80	21.63	19.54	14.23	18.66	14.65	13.45	37.64
120	33.17	26.44	22.93	25.88	26.81	22.56	51.64
160	42.99	38.62	31.56	36.42	35.6	31.28	68.75
200	55.12	51.34	45.36	50.88	45.84	44.62	79.45
240	66.67	61.76	55.48	58.53	56.43	54.29	88.67

Figures:

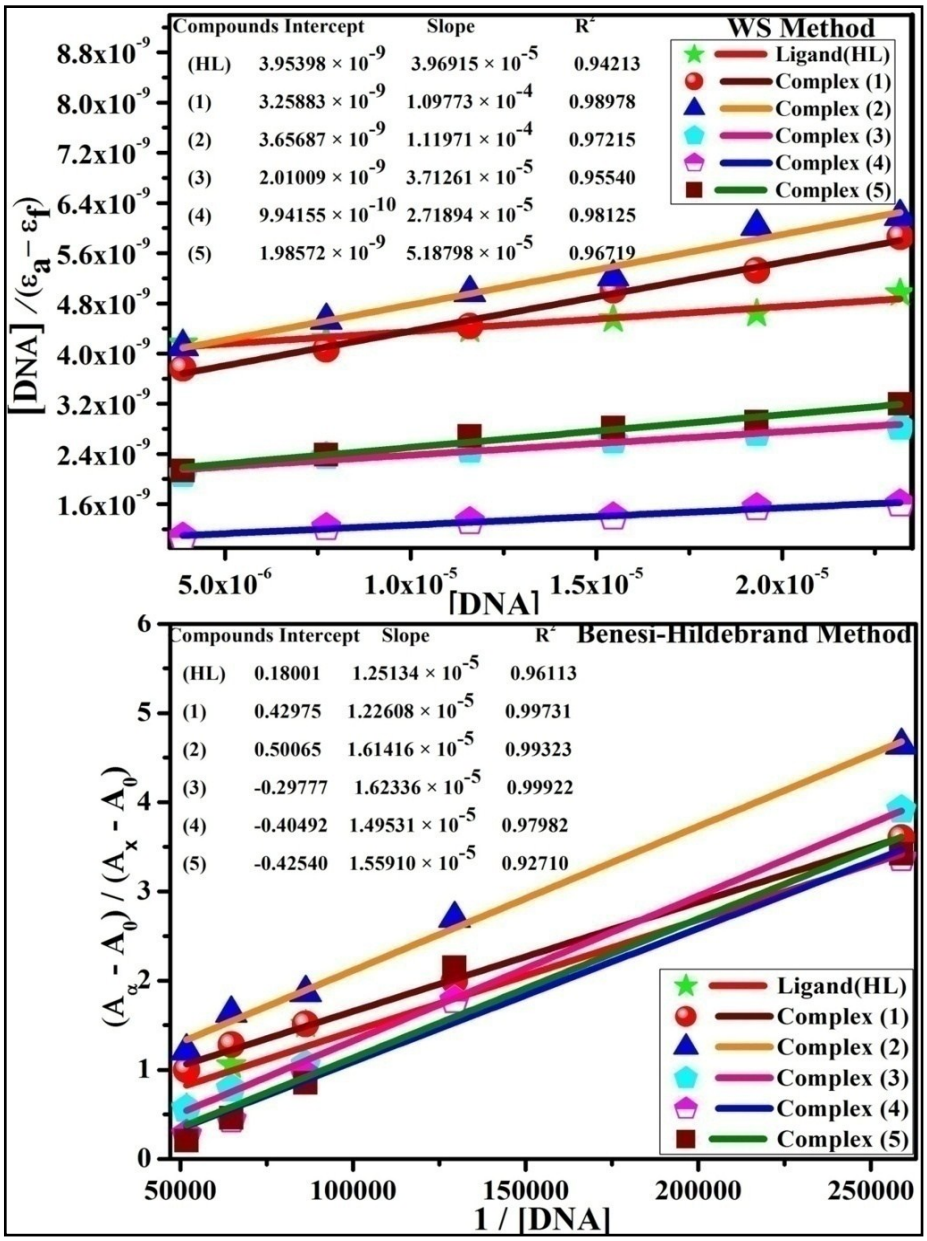

Fig. S12. Linear plots of {[DNA] / (ε_a - ε_f)} versus [DNA] M by Wolfe-Shimmer method and [(A_∞ - A_0) / (A_x - A_0)] versus {1 / [DNA]} M^{-1} by Benesi-Hildebrand method for the estimation of the intrinsic DNA binding constants (K_b).

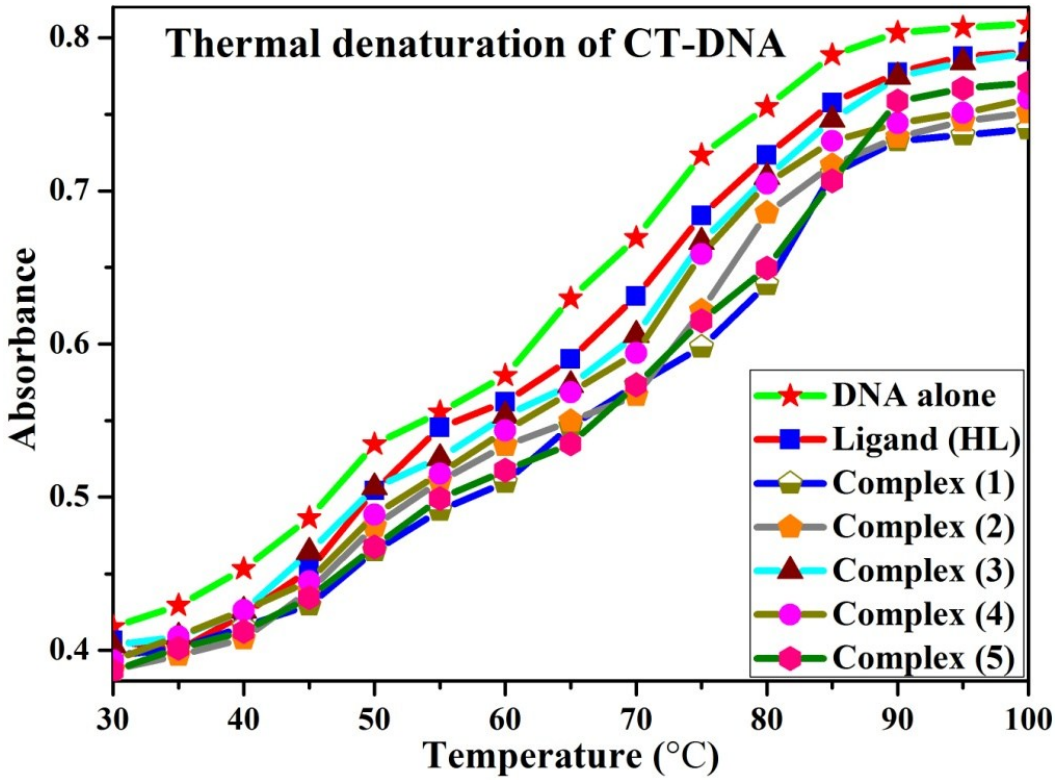

Fig. S13. DNA thermal denaturation profile in the absence and presence of compounds in Tris-HCl buffer pH = 7.2, [DNA] / [Complex] = 1 ratio.

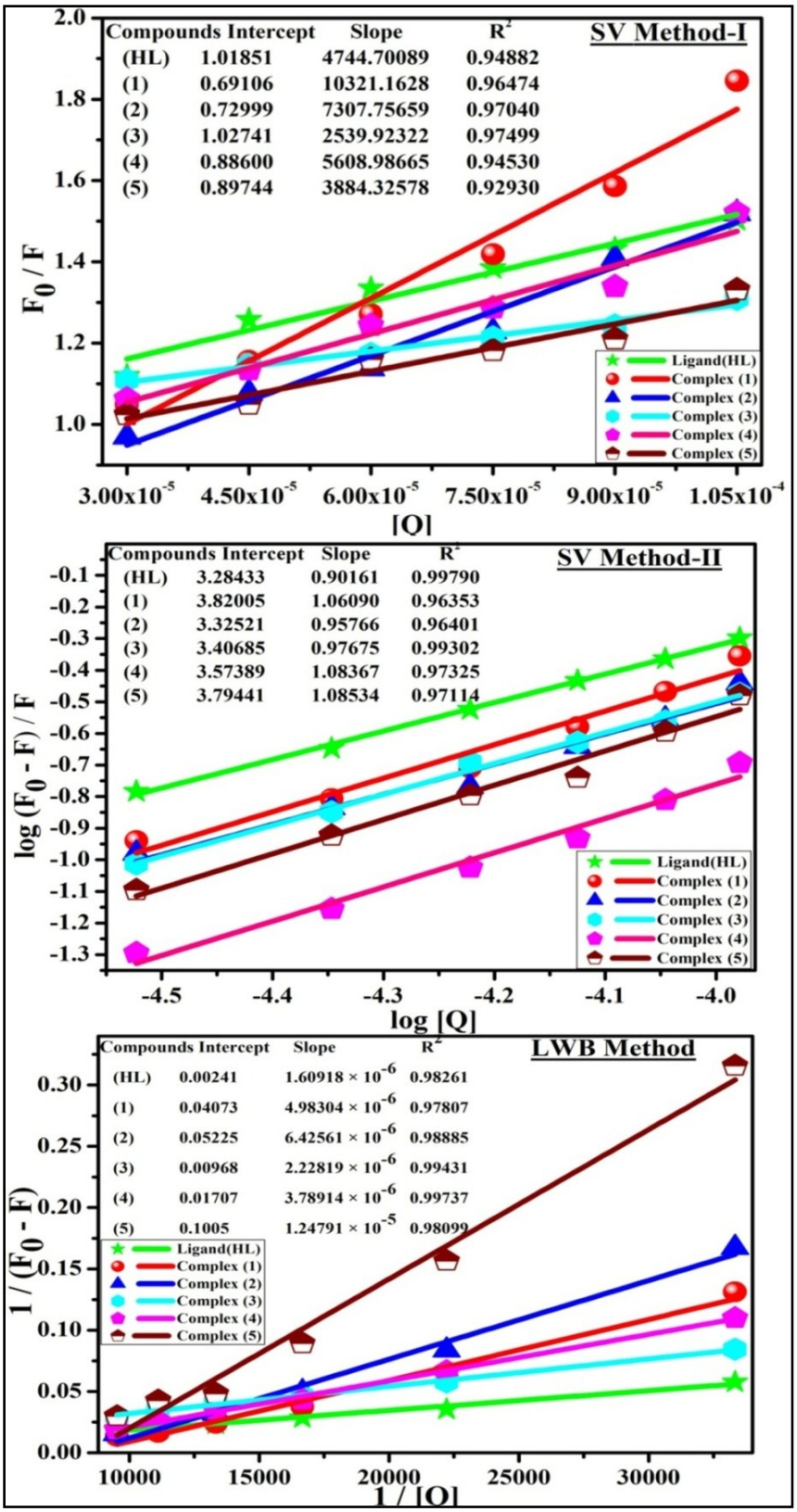

Fig. S14 Stern-Volmer linear plots of F_0 / F *vs* [Q] (Method-I), F_0 / F *vs* [Q] (Mehod-II) and Lineweaver-Burk linear plot of 1/ (F_0–F) *vs* 1/ [Q] for the quenching of fluorescence of ethidium bromide (EB)-DNA complex caused by ligand (**HL**) and complexes (**1-5**).

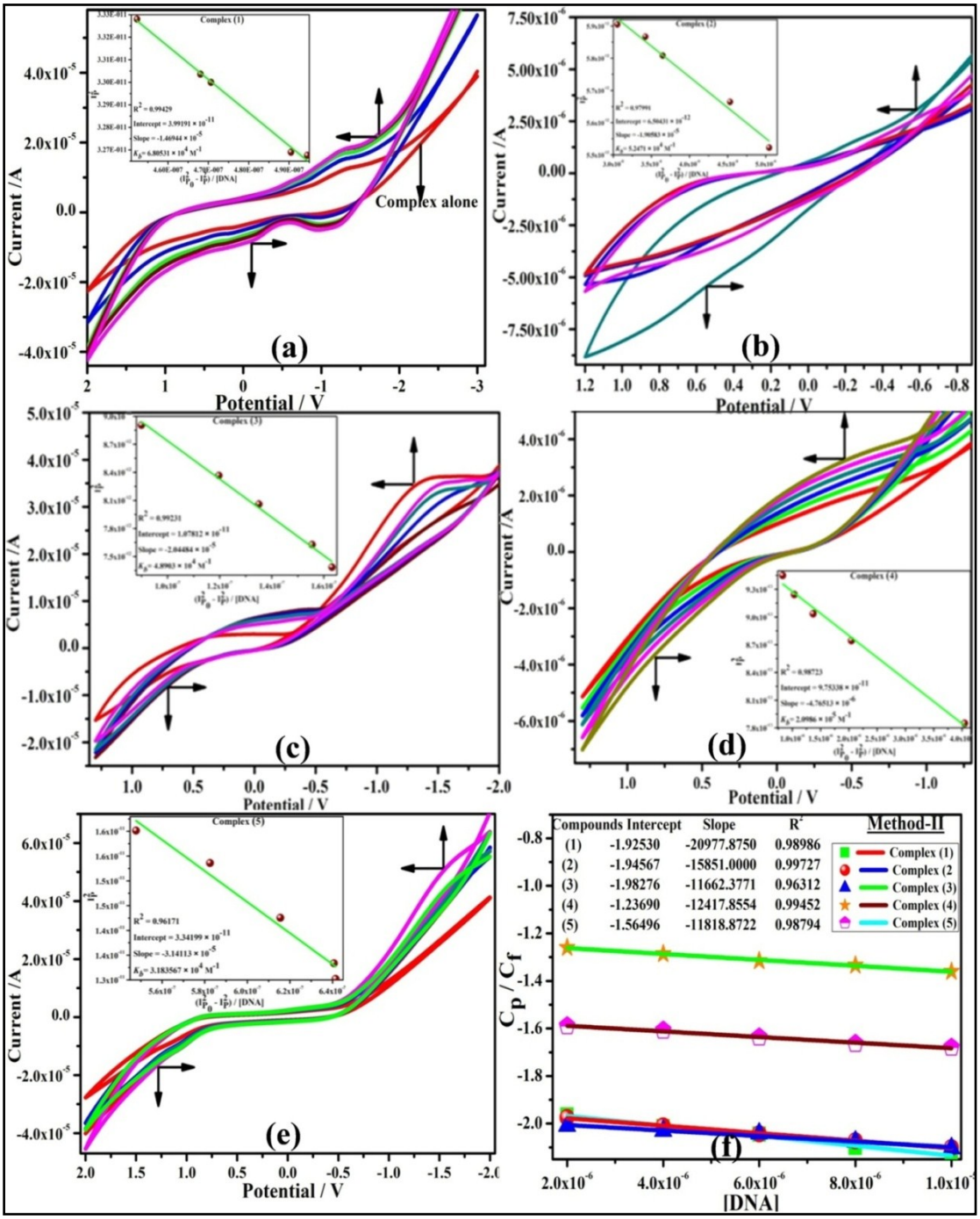

Compounds	Intercept	Slope	R^2
(1)	-1.92530	-20977.8750	0.98986
(2)	-1.94567	-15851.0000	0.99727
(3)	-1.98276	-11662.3771	0.96312
(4)	-1.23690	-12417.8554	0.99452
(5)	-1.56496	-11818.8722	0.98794

Fig. S15 Cyclic voltammograms of complexes (**1-5**) (**a-e**) in Tris-HCl buffer pH = 7.2 at 25 °C in presence of increasing amount of DNA and arrow indicates the changes in peak current and potentials at scan rate 100 mvs^{-1}. Inset: The calculated binding constant (K_b) from linear plot of Ip^2 *vs* ($I_{po}^2 - I_p^2$) / [DNA] by Method-I and the linear plots for all complexes of C_p / C_f *vs* [DNA] by Method-II.

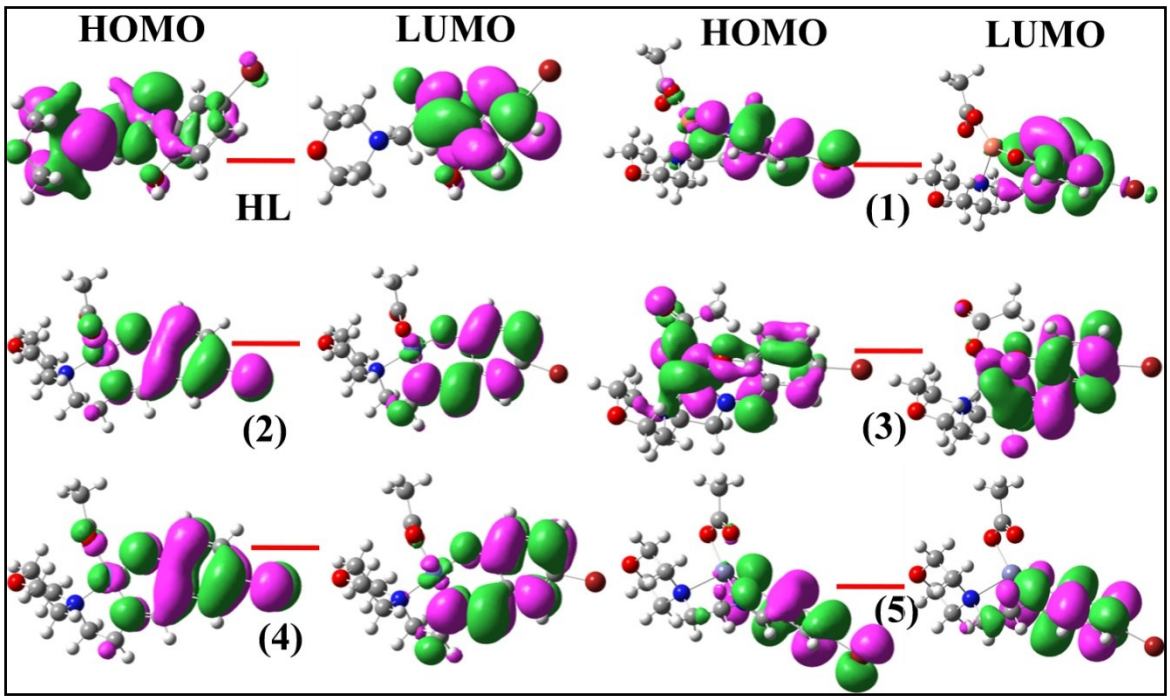

Fig. S16 Frontier molecular orbitals (HOMO and LUMO) of ligand (**HL**) and its complexes (**1-5**) from DFT calculations.

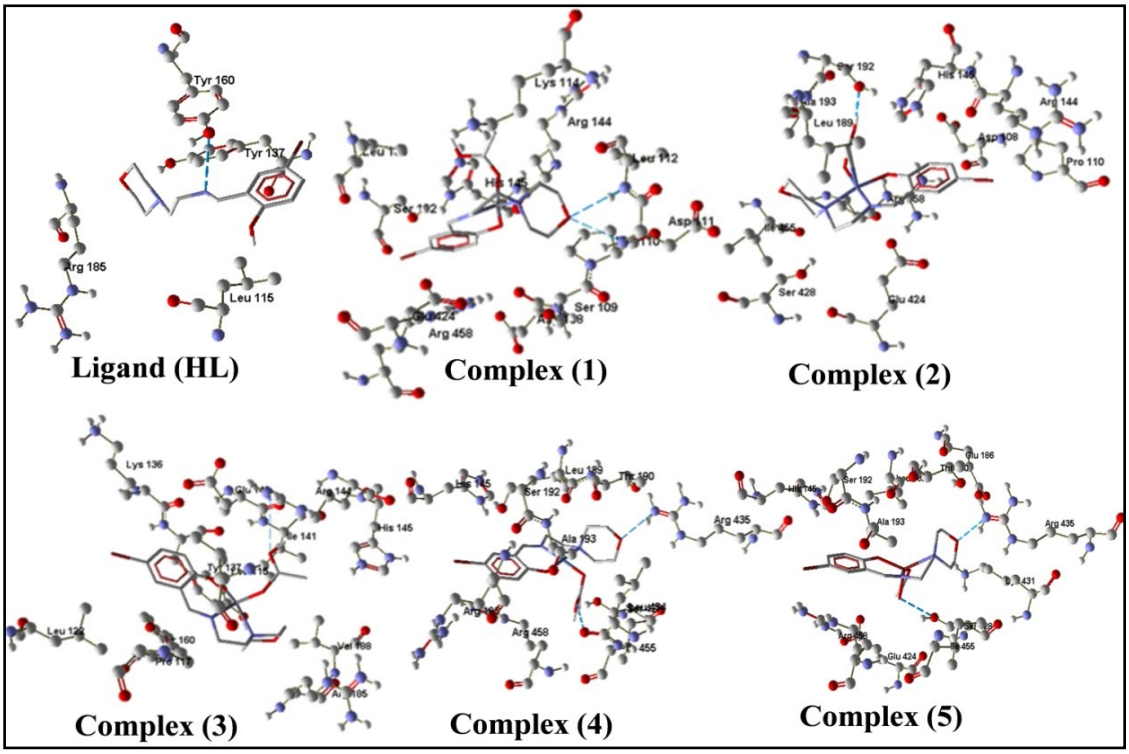

Fig. S17 Key interactions in the active site of ligand (**HL**) and its complexes (**1-5**) bound BSA protein obtained from molecular docking studies. (For clarity, the hydrogen atoms are omitted and hydrogen bonding is indicated by dotted line)

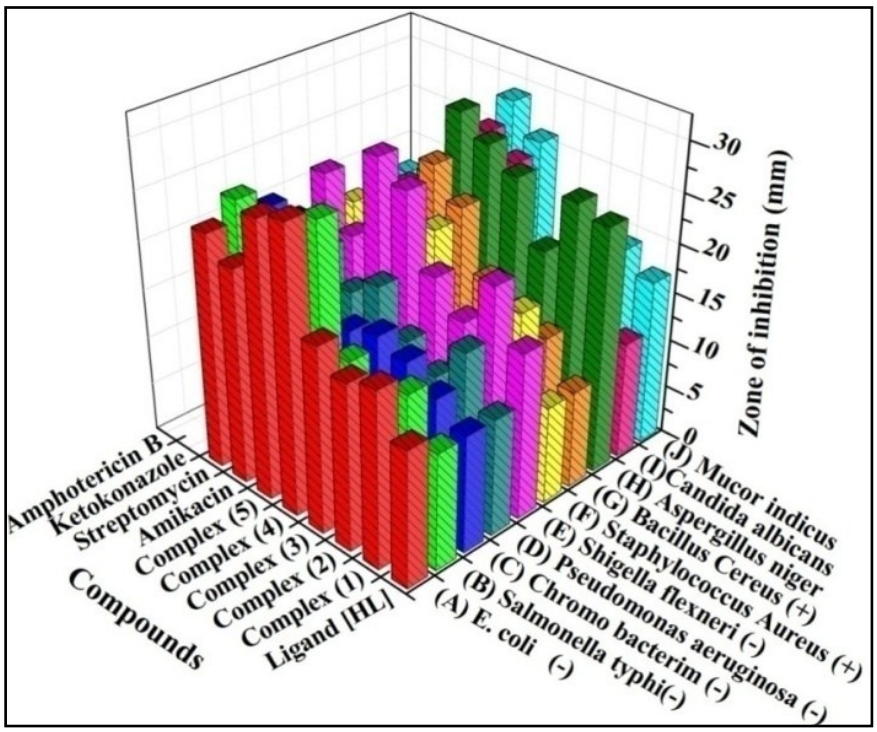

Fig. S18 Histogram showing the comparative antimicrobial activities of ligand (**HL**) and its complexes (**1-5**) by Agar disc diffusion method.

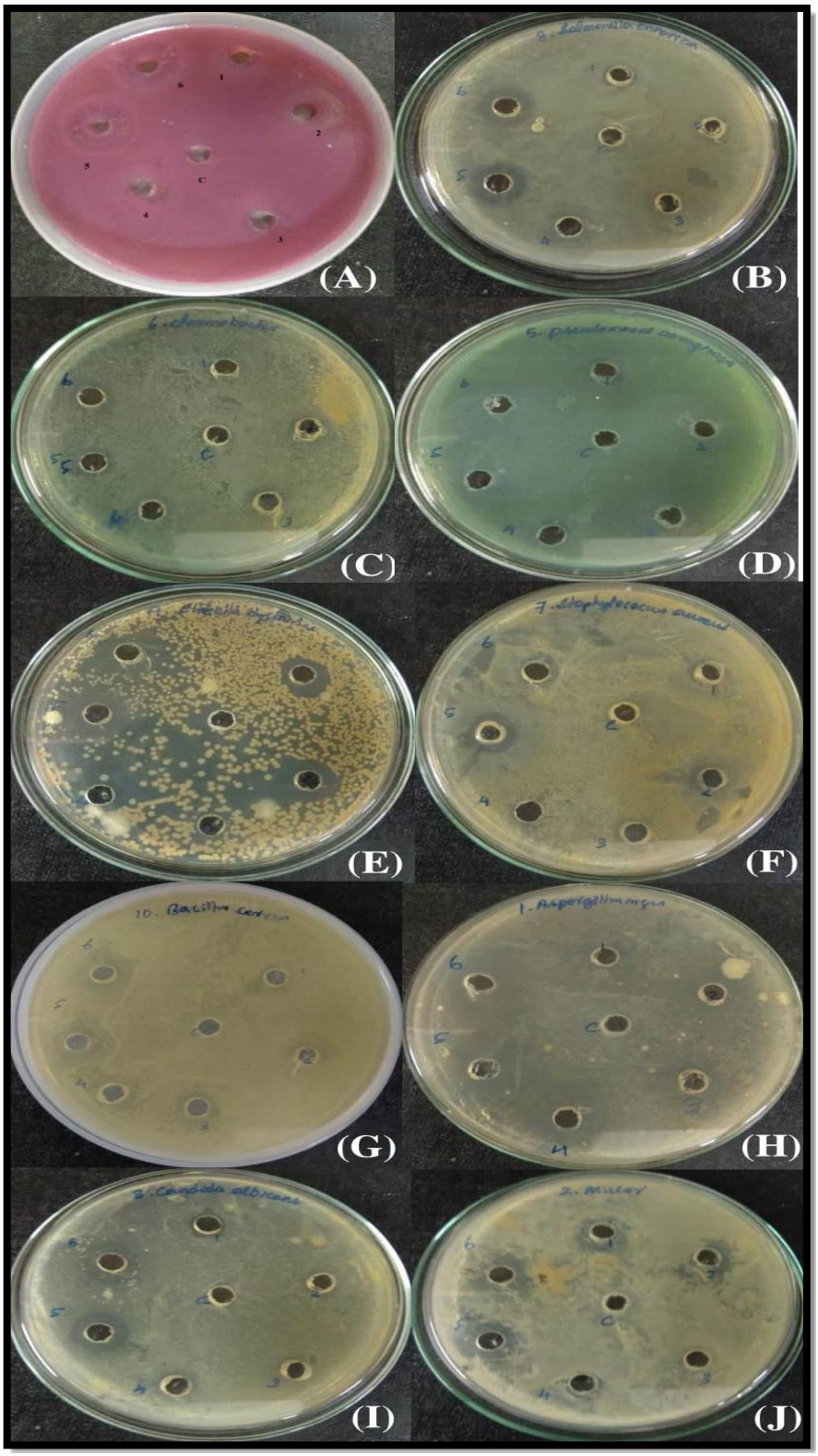

Fig. S19 Antibacterial and antifungal activities of ligand (**HL**) and its complexes (**1-5**) by Agar disc diffusion method, plates (**A-J**) well no: C-Control (DMSO solvent), 1. Ligand (**HL**), 2. Complex (**1**), 3. Complex (**2),** 4. Complex (**3),** 5. Complex (**4)** and 6. Complex (**5).**

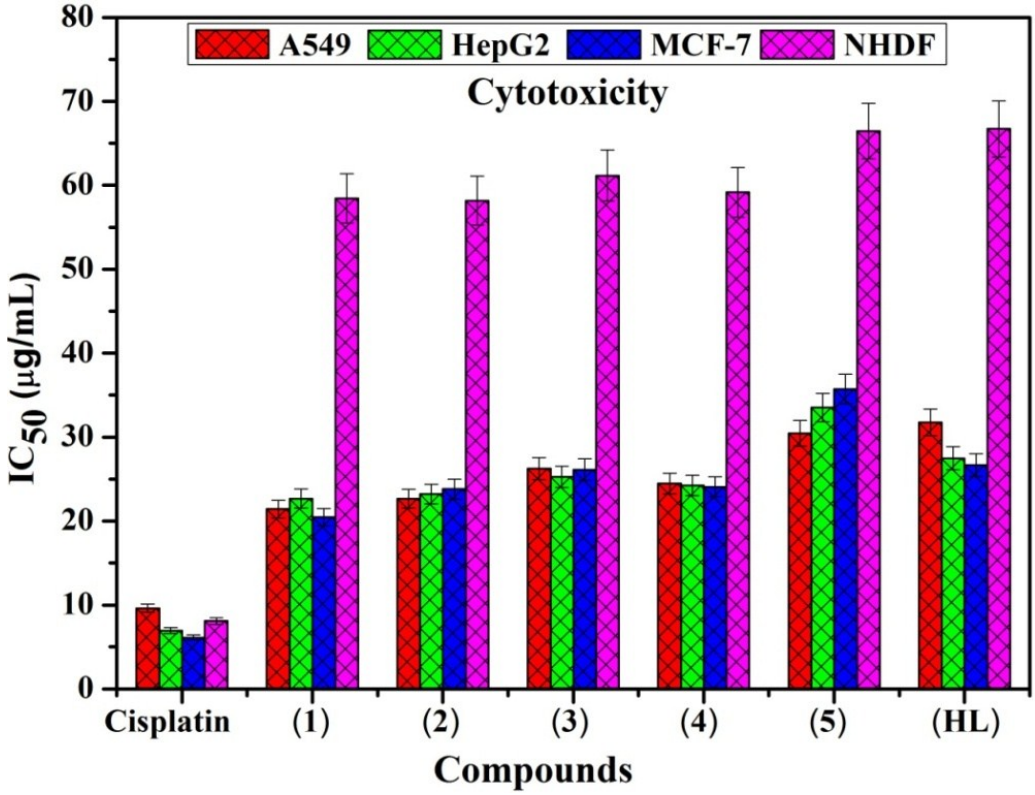

Fig. S20 The comparison of cytotoxic effects of ligand (**HL**) and complexes (**1-5**) with standard drug cisplatin against axenic cancer and normal cell lines.